5

Power Quality Recognition in Distribution System with Renewable Energy Penetration: Simulation Approach

Experimental results presented in the chapter 4 indicate that the PQ events are associated with outage and grid synchronization of wind generator and solar PV system. However, due to limitations of the experimental set-ups, the detailed study is needed in this field. Hence, this chapter has considered detailed study of detection of islanding, outage of wind/solar generators, grid synchronization of wind/solar generators and analysis of the PQ disturbances associated with these events.

5.1 INTRODUCTION

Integration of the renewable energy (RE) sources such as solar photovoltaic (PV) system and wind energy into the utility grid is gaining momentum due to their potential benefits in reducing carbon emissions, improving energy efficiency and reliability of power supply [Hong et al., 2016]. Loss in sustainability of the conventional power sources also forced the utilities to increase penetration level of RE sources. Recently, the wind energy and solar PV systems are recognized as one of the most mature and fastest growing renewable energy (RE) technology. According to the data published by the Global wind energy council (*GWEC*), the wind industry is growing continuously worldwide and the total installed wind capacity has reached 318 GW at the end of 2013 [Yang and Tian, 2015]. Penetration level of the solar PV energy into the utility grid has increased considerably, with remarkable growth since 2005. The integration of solar PV energy and wind energy into the existing distribution and transmission networks presents technical challenges in terms of stability, reliability, protection, voltage regulation, safety issues and power quality (PQ) problems [Ray et al., 2013]. Increase in penetration level of the distributed generation (DG) sources like wind, solar, and fuel cell into the utility grid increases the power quality problem [Somayajula and Crow, 2014]. Harmonic distortions, voltage unbalance, voltage sag, voltage swell, notch, momentary interruption and flicker are recognized as power quality problems associated with modern variable wind speed turbines [Abrantes, 2012]. Power quality issues associated with these turbines are determined on the basis of measurements and norms as specified in the International Electro-Technical Commission standard, IEC-61400 [Mohod and Aware, 2010]. Operational events of wind generator and solar PV system influence power quality (PQ) of distribution networks. Large current variations during outage and synchronization of solar PV system can lead to significant voltage transients [Mohanty et al., 2013]. A detailed study of current unbalance in the grid connected building integrated solar PV systems is provided in [Chicco et al., 2014]. Power quality parameters, of power output of a Solar PV Power Plant are governed by relevant IEC Standards such as IEC 60904, 61850.

The signal processing and artificial intelligence techniques are applied for detection of PQ disturbances associated with distributed generation (DG). Ray *et al.* [Ray et al., 2014], proposed a hyperbolic S-transform based classifier employing support vector machine (SVM) and decision tree (DT) for the detection and classification of PQ disturbances in the distributed generation systems. Power quality analysis of a large wind power generation system integrated with the practical

distribution network of Taiwan has been presented by authors in [Hsu et al., 2015]. The WT and ST based approach for detection of different PQ disturbances in grid-connected wind power system has been proposed by the authors in [Ray et al., 2010]. Power quality assessment of 3-phase grid connected solar PV system with single and dual stage circuits has been presented in [Patra et al., 2016]. Rahmani *et al.* [Rahmani et al., 2015], presented an advanced universal power quality conditioning system and hybrid maximum power point tracking (MPPT) method to interface solar PV systems to the power system network addressing power quality.

In this chapter a technique for the detection of various operational events in the RE sources based power system is proposed. Features extracted using *S*-transform based multi-resolution analysis of the negative sequence component of voltage captured at the point of common coupling (PCC) are used for the detection of these events. This chapter has considered S-transform for detection of power quality disturbances in distribution system associated with operations of wind generator and solar PV system such as synchronization, outage and islanding of test system from the utility grid. Effects of wind speed and solar insolation variations on the power quality have also been investigated. Power quality assessment in the hybrid power system is also carried out. Different plots obtained from the *S*-transform based multi-resolution analysis have been utilized for the detection of PQ disturbances. Power frequency variations and total harmonic distortions of voltage and current signals have also been considered. Proposed power quality index (PQI) has been used to investigate the impacts of high wind and solar energy penetration on the power quality. Study has been carried out using MATLAB/Simulink and the simulation results are compared with the real time results obtained by the use of real time digital simulator (RTDS) for testing the effectiveness of proposed approach.

5.2 PROPOSED TEST SYSTEM

This section describes the configuration of RE sources based power system utilized for the study. The wind energy conversion system and solar PV system are also presented in detail.

5.2.1 IEEE-13 Bus Test Feeder

Proposed study is carried out using a modified IEEE-13 bus test system. The original system is a grid connected 60 Hz, 5 MVA radial distribution feeder with two voltage levels of 4.16 kV and 0.48 kV feeding balanced and unbalanced loads with no RE sources [Kersting, 1991]. This test feeder is modified to incorporate the wind generator, solar PV system, diesel generator and balanced loads as shown in Fig. 5.1. The load parameters are provided in Table 5.1. The distributed load between nodes 632 and 671 is replaced by a spot load placed at middle of the feeder. All the system feeders are three phase with three phase balanced loads where considered. Test feeder is connected to the utility grid through a Substation transformer (*SST*). Transformer connected between the nodes 633 and 634 is designated as XFM-1. In Indian power system, the renewable energy (RE) sources are installed at remote locations where land is easily available and connected to the transmission network through local network developed for RE sources. The first wind generator (WG-1) is connected to the node 680 via transformer XWG-1 and second wind generator (WG-2) is connected to the node 646 via transformer XWG-2 with the help of circuit breakers CB2 and CB5 respectively. Capacity of each wind generator used in the proposed study is 1.5 MW. The diesel generator of capacity 3.125 MVA is connected to the node 632 via transformer XDG with the help of circuit breaker CB4. The $100kW$ solar PV plant is connected on the bus 680 through a transformer XSPV and 5 km long overhead transmission line with the help of circuit breaker CB3. The transmission line has the positive and zero sequence resistances of 0.1153 and $0.413ohm/km$, positive and zero sequence inductances of $1.05e^{-3}$ and $3.32e^{-3}H/km$, and positive and zero sequence capacitances of $11.33e^{-9}$ and $5.01e^{-9}F/km$ respectively. Effect of high solar energy penetration on the power quality has been investigated with the help of $500kW$ and $1MW$ solar PV systems inte-

grated at bus 680 through the above mentioned transformer (XSPV) and a transmission line. The transformer data are provided in Table 5.2. Voltage regulator (*VR*) between nodes 650 and 632 in original system is realized by On load tap changer (*OLTC*) transformer. The switch between nodes 671 and 692 is realized by three phase circuit breaker. Load L comprising of 500*kW* active and 500*kVAr* reactive powers is connected on bus 680 using circuit breaker CB1 is used for the study of grid disturbances due to operation of load. For islanding operation of the test system, an Island interconnection device (*IID*) is connected between utility grid and node 650.

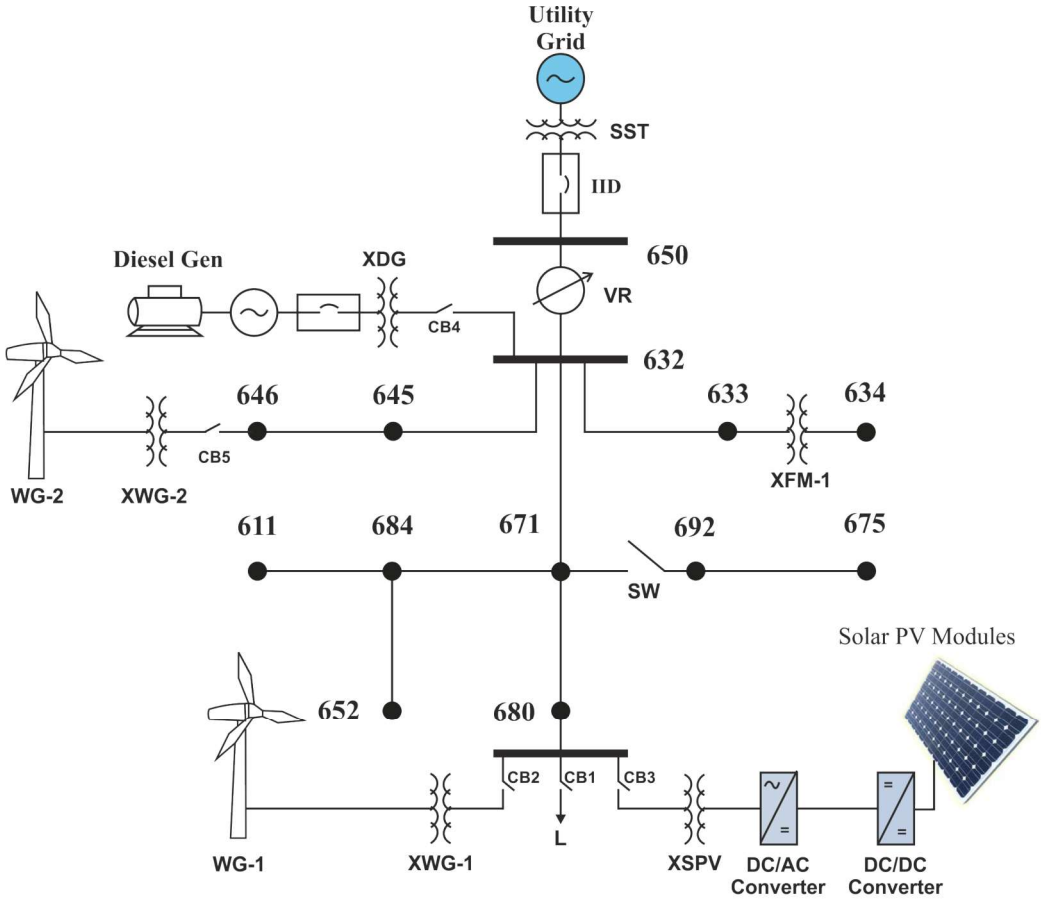

Figure 5.1 : Modified IEEE-13 bus test system

All the feeders are three phase with three phase balanced loads where considered. The aerial feeders use configuration 601 with phase conductor type 556, 500, 26/7 ACSR and neutral conductor type 4/0, 6/1 with spacing ID 505, while the underground cables use configuration 606 with conductor 250, 000 AA, CN with spacing ID 515. According to the type of conductors and topology of the feeders, the series impedance matrices of the feeder configurations 601 (Z_{601}) and 606 (Z_{606}) in Ω/km are given by the following relations [Paz et al., 2010].

$$Z_{601} = \begin{bmatrix} 0.2153 + j0.6325 & 0.0969 + j0.3117 & 0.0982 + j0.2632 \\ 0.0969 + j0.3117 & 0.2097 + j0.6511 & 0.0954 + j0.2392 \\ 0.0982 + j0.2632 & 0.0954 + j0.2392 & 0.2121 + j0.6430 \end{bmatrix} \tag{5.1}$$

Table 5.1 : Loading and Generator Status of Test System

Bus	Load Model	Load		Capacitor banks	Generator
		kW	kVAr	kVAr	
634	Y-PQ	400	290		
645	Y-PQ	170	125		
646	Y-PQ	230	132		WG-2
652	Y-PQ	128	86		
671	Y-PQ	1155	660		
675	Y-PQ	843	462	600	
692	Y-PQ	170	151		
611	Y-PQ	170	80	100	
632-671*	Y-PQ	200	116		
680		L			WG-1, SPV system
650					Utility grid
632					Diesel Generator

⋆ Distributed load between nodes 632 and 671 is replaced by spot load placed at middle of the line

Table 5.2 : Transformer Data of Test System

Transformer	MVA	kV-High	kV-Low	HV Winding		LV Winding	
				R(Ω)	X(Ω)	R(Ω)	X(Ω)
Substation	10	115	4.16	29.095	211.60	0.1142	0.8306
XFM-1	5	4.16	0.48	0.3807	2.7688	0.0510	0.0042
XWG-1	5	4.16	0.575	0.3807	2.7688	0.0510	0.0042
XWG-2	5	4.16	0.575	0.3807	2.7688	0.0510	0.0042
XDG	5	4.16	2.40	0.3807	2.7688	0.0510	0.0042
XSPV	1	4.16	0.260	0.1730	195.70	0.0007	0.7645

$$Z_{606} = \begin{bmatrix} 0.4960 + j0.2773 & 0.1983 + j0.0204 & 0.1770 + j0.0089 \\ 0.1983 + j0.0204 & 0.4903 + j0.2511 & 0.1983 + j0.0204 \\ 0.1770 + j0.0089 & 0.1983 + j0.0204 & 0.4960 + j0.2773 \end{bmatrix} \tag{5.2}$$

The positive and zero sequence capacitances for configuration 601 are 1.57199 nF/km and 1.3398 nF/km respectively whereas for configuration 606 both positive and zero sequence capacitances are equal to 15.96979 μF/km. Length of the line segments is same as in the original test feeder. The feeder characteristics are provided in Table 5.3.

5.2.2 Wind Energy Generation System

Block diagram of the proposed grid connected wind energy conversion system (WECS) is illustrated in Fig. 5.2. It consists of a doubly fed induction generator (DFIG) interfaced to an IEEE-13 bus test feeder utilizing the rotor side converter, grid side converter, filter and a transformer.

The wind energy conversion system used for recognition of PQ disturbances is consists of a doubly fed induction generator driven by a wind turbine. The DFIG consists of a wound rotor

Table 5.3 : Feeder Data of Test System

Bus A	Bus B	Length (m)	Configuration
632	645	152.4	601
632	633	152.4	601
633	634	0	XFM-1
645	646	91.44	601
650	632	609.6	601
684	652	243.84	606
632	671	609.6	601
671	684	680	601
671	692	0	Switch
684	611	91.44	601
692	675	152.4	606

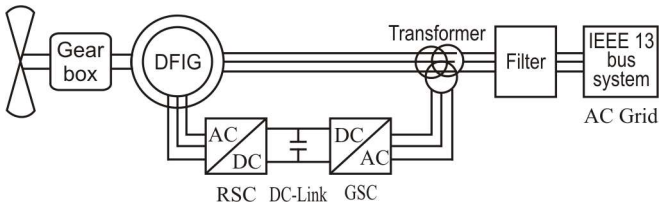

Figure 5.2 : Block diagram of proposed grid connected wind energy conversion system

and an adjustable speed Induction generator (*IG*). This generator provides high energy yields, reduction of mechanical loads, simpler pitch control, less fluctuations in output power, an extensive controllability of both active and reactive powers [Li et al., 2010]. A detailed description of wind profile, wind energy conversion system, wind generators and their power electronics converters, and international grid codes used for the grid integration of wind energy has been reported in [Mahela and Shaik, 2016a]. Stator of the DFIG is connected to the IEEE-13 bus test system through transformer and filter while the rotor is connected through the rotor side converter (RSC), the dc-link, the grid side converter (GSC) and a filter. Converter enables decoupled control of active and reactive power of DFIG, moreover the reactive power control can be achieved at lower cost because DFIG operates similar to a synchronous generator [Ehlert and Wrede, 2007]. The control for both RSC and GSC is implemented using proportional-integral (PI) controller based back-to-back PWM converter.

(a) Wind turbine

Wind turbine (WT) has blades connected to the mechanical shaft through gearbox and rotor hub. It converts kinetic energy of the wind into mechanical energy of the shaft. The shaft drives the generator to convert mechanical energy into electrical energy. The energy contained by wind depends on wind velocity (v) and air density (ρ). The output mechanical power developed by the WT can be expressed by the following relation [Thomas and Cheriyan, 2012]:

$$P_m = \frac{1}{2}\rho A v^3 C_p(\lambda, \beta) \tag{5.3}$$

where A is the area swept by rotor blades; C_p is the power coefficient (or coefficient of performance) of wind turbine which is a non-linear function of tip-speed ratio λ and the blade pitch angle β.

(b) Drive Train System

The drive-train system of a WECS comprises of the wind wheel, the turbine shaft, the gear-box, and the generator's rotor shaft. The wind wheel inertia is usually about 90% of inertia of the whole system and gearbox usually has a multiplication ratio between 50 and 100. The gearbox transfers aerodynamic power from the slow rotating turbine shaft to the fast rotating mechanical shaft which drives the generator. The gear ratio (GR) is defined by the relation [Kamel, 2014]:

$$GR = \frac{\omega_g}{\omega_m} \tag{5.4}$$

where ω_g is the generator speed in (rad/s). Mathematical modelling using single-mass system is given by the following relation:

$$T_m = J_{eq}\frac{d\omega_m}{dt} + B\omega_m + T_e \tag{5.5}$$

where T_m is the turbine driving torque; J_{eq} is the total equivalent inertia of turbine and generator; B is the damping coefficient representing generator and turbine rotational losses; T_e is the electro-magnetic torque of the generator; ω_m is the rotor mechanical speed. The rotor mechanical speed is related to the rotor angular speed of the electric machine (ω_g) through the following relation.

$$\omega_m = \frac{\omega_g}{n_p} \tag{5.6}$$

with n_p being the number of pole-pairs of the generator.

(c) Control Parameters for Wind Turbine

The proportional integral (PI) controller is used for converter used to integrate the wind generator to the test grid. The output of PI controller ($u(t)$) can be defined by the following equation.

$$u(t) = K_p e(t) + K_i \int (\tau) d\tau \tag{5.7}$$

with K_p is the proportional gain, K_i is the integral gain, t is the instantaneous time and $e(t)$ is the error and τ is the variable of integration (takes on values from time 0 to t).

Frequencies of grid side and rotor side PWM carriers are 2700 Hz and 1620 Hz respectively. Maximum pitch angle is 27° and maximum rate of change of pitch angle is 10°/s. Pitch controller gain is 150. Reactive power and voltage regulator gains are 0.05 and 20 respectively. Various Kp and Ki gains are given in Table 5.4. Control techniques are not described in detail due to the page limitation as the main concern of the study is wind operations and not the control techniques.

(d) Wind Generator Data

The wind generators WG-1 and WG-2 each of capacity 1.5 MW, 575 V, 60 Hz are connected to buses 680 and 646 respectively of an IEEE-13 bus test system. The rated wind speed is 11 m/s.

Table 5.4 : Kp and Ki Controller Gains of WECS

Element	Kp	Ki
DC bus voltage regulator	8	400
Grid side converter current regulator	0.83	5
Rotor side converter current regulator	0.86	8
Speed regulator	3	0.6
Pitch compensation gains	3	30

Other generator data (for each generator) are as follows: H (inertia constant)= 0.685 s, R_s=0.023pu, L_s=0.18pu, R_r= 0.016pu, L_r= 0.016pu, L_m=2.9pu.

5.2.3 Solar Photovoltaic System

Block diagram of the proposed solar PV system is illustrated in Fig. 5.3. It consists of a solar PV array interfaced to an IEEE-13 bus test feeder through the power electronics converter system consisting of a DC-DC boost converter, an inverter, a filter and a transformer (XSPV).

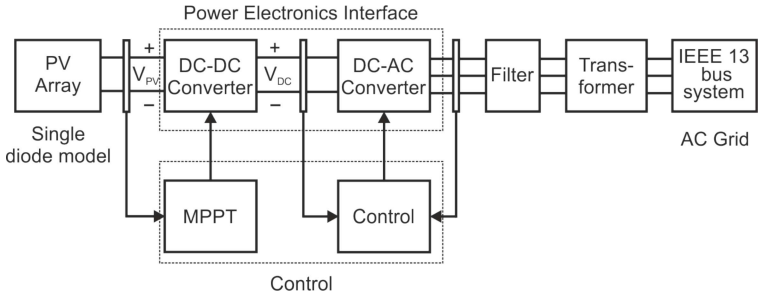

Figure 5.3 : Block diagram of grid-connected solar PV system

(a) PV Array Model

The solar PV plant of capacity 1MW consists of 10 units each of capacity 100kW connected in parallel whereas such 5 units are connected in parallel to form a solar PV system of capacity 500kW. Each solar PV unit of 100kW consists of an array consisting of 66 parallel strings. In this array each string has 5 modules connected in series and each module has 96 solar cells. Solar cell consists of a p-n junction fabricated in a thin layer of semiconductor like a p-n junction diode. An electrical equivalent circuit of a solar cell can be represented by a single or double diode model. Single diode equivalent model has simplicity with sufficient accuracy [Kuo et al., 2013]. Hence, the single diode equivalent circuit with parallel and series resistances as shown in Fig. 5.4, has been utilized in the proposed study.

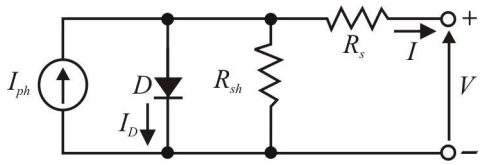

Figure 5.4 : Single-diode equivalent circuit of a solar cell

Relationship between output voltage (V) and output current (I) for single-diode equivalent circuit of a solar cell can be described by the following relation [Ding et al., 2012]

$$I = I_{ph} - I_0 \left\{ exp\left[\frac{q(V + IR_{spv})}{A_c k_b T}\right] - 1 \right\} - \left(\frac{V + IR_{spv}}{R_{sh}}\right) \tag{5.8}$$

where I_{ph} is the PV cell photo-current, I_0 is the PV cell saturation current, A_c is the curve fitting factor of a solar cell, R_{sh} is the PV cell shunt resistance, R_{spv} is the PV cell series resistance, q is the electron charge (1.602×10^{-19}C), and k_b is the Boltzmann constant ($1.38\times10^{-23}\ J/K$).

The value of R_{sh} can be assumed to be infinite at short circuit conditions, where slope of the I-V characteristics is almost zero [Ding et al., 2012]. In this case, I_{ph} is equal to the short circuit current (I_{sc}) [Kuo et al., 2013]. For a PV array arranged in N_p parallel and N_{s1} series connected solar cells is given by the following relation.

$$I = N_p I_{sc} - N_p I_0 \left\{ exp\left[\frac{q(V + I(N_{s1}/N_p)R_{spv})}{N_s A_c k_b T}\right] - 1 \right\} \tag{5.9}$$

Parameters used in the proposed study at Standard test conditions (STC) for each module are as $V_{oc} = 64.2V$, $I_{sc} = 5.96A$, $V_{mp} = 54.7V$, $I_{mp} = 5.58A$, $R_{spv} = 0.037998\Omega$, $R_{sh} = 993.51\Omega$, $I_0 = 1.1753e^{-8}A$, diode quality factor Q_d=1.3, and $I_{ph} = 5.9602A$. V_{mp} and I_{mp} are respectively the voltage and current corresponding to maximum power point tracking whereas V_{oc} represent the open circuit voltage of solar module.

(b) Power Electronics Interface

Practically, the output voltage of one PV string is very low despite the use of MPPT. This requires the use of front end dc-dc boost converter for integrating the low voltage PV modules to the utility grid. It also performs the function of MPPT under the nominal utility conditions [Jou et al., 2015]. An inverter converts the DC output power of boost converter into 50 or 60 Hz AC power. In the proposed study the DC-DC boost converter increases DC output voltage of the solar PV array from $273.5V$ to $500V$ and DC-AC inverter converts $500V$ dc to $260V$, $60Hz$, three phase ac supply. Switching frequency of the boost converter is $5kHz$. The inverter action is provided by a 3-level voltage source converter with switching frequency of $19.8kHz$. Transformer $XSPV$ with voltage ratio 0.260/4.16 kV is used as an isolation transformer between the inverter and IEEE-13 bus test system. Control methods are not discussed in detail due to page limitations as the main concern of the study is related to the grid phenomenon and not to control techniques. Control of the DC-DC boost converter is provided using incremental conductance and integral regulator based MPPT technique of the solar PV system. Detailed description of the incremental conductance method can be found in the references [Ram et al., 2017]. The dq frame pulse-width modulation (PWM) control strategy has been employed for the control of inverter of the solar PV system. Detailed description of this control strategy is reported in the references [Areerak et al., 2008; Ibarra et al., 2015].

(c) Filter

A filter consisting of inductance and capacitance (LC filter) is used between inverter and the grid. Filter is designed to reduce higher-order harmonics introduced due to PWM modulation of the DC/AC converter. A filter with series branch having resistance of $2m\Omega$ and inductance of $0.25mH$, and shunt capacitor branch of $100kVar$ are used at the output terminals of inverter to filter out the harmonic components.

5.3 PROPOSED METHODOLOGY FOR DETECTION OF OPERATIONAL EVENTS

Block diagram shown in Fig. 5.5 depicts the algorithm used for detection of operational events like islanding, outage and grid synchronization of RE sources. The voltage signal captured

at bus 650 is analysed into sequence components through a sequence analyser. Among these sequence components, negative sequence component is found to be useful in identifying various operational events. This negative sequence voltage is sampled at $1.92kHz$ i.e. 32 samples per cycle and is decomposed using *S*-transform to obtain *S*-matrix. Statistical features extracted from *S*-matrix are designated by F1 and F2 as defined below.
F1: Kurtosis of sum absolute values of *S*-matrix.
F2: Maximum value of variance of *S*-matrix.

The operational events are classified with the help of above mentioned features as detailed below.

- Feature F1 is used to classify the operational events into two groups by comparing the threshold value TH1. The operational events with F1 <TH1 are grouped as synchronization events whereas the outage and islanding events will have F1 >TH1.
- The outage and islanding events are further classified with the help of feature F2 by comparing the threshold value TH2. The outage events will have F2 <TH2 whereas the islanding events will have F2 >TH2.
- The feature F2 is used to identify the operational events of a particular group of RE sources present during an event.
- Succeeding section of the chapter presents the PQ assessment during the different operational events in the hybrid power system.

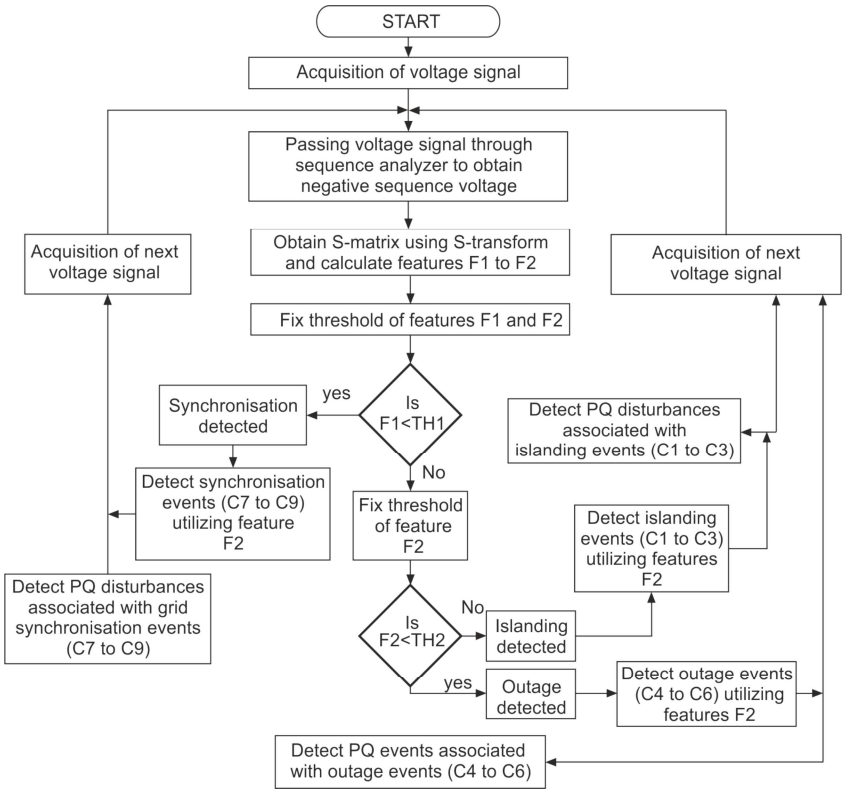

Figure 5.5 : Flow chart for detection of islanding, outage and synchronization events

5.4 PROPOSED METHODOLOGY FOR DETECTION OF POWER QUALITY DISTURBANCES ASSOCIATED WITH OPERATIONAL EVENTS

Block diagram of the proposed algorithm for detection of PQ events is shown in Fig. 5.6. Following steps are used in the proposed algorithm for investigation of PQ events:

- Voltage signal is captured at bus 650 of the test system. Current injected by the solar PV system and wind energy conversion system into the utility grid are also captured.
- Voltage signal is decomposed using multi-resolution analysis based on *S*-transform and *S*-matrix is obtained. The sampling frequency of 1.92 kHz i.e. 32 samples per cycle for 60 Hz frequency is used.
- Plots such as time-frequency contour (*S*-contour), amplitude-time curve, sum absolute values-time curve, phase curve and amplitude-frequency curve are obtained from the *S*-matrix corresponding to each case study. The *S*-contour provides information regarding the time localization of time-series data. Parameters are normalized with respect to maximum values.
- Proposed sum absolute values curve is obtained by the sum of absolute values of each column of the *S*-matrix. This enhances performance of the proposed algorithm and clearly shows the presence and location of each PQ disturbance available in the signal.
- PQ recognition results have been obtained from the analysis of *S*-transform based plots.
- Total harmonic distortions of voltage (THD_v) and current (THD_i) are obtained using FFT and considered for PQ analysis.
- Power frequency variations have been detected directly by monitoring the system frequency. Maximum deviations in the frequency are considered for PQ recognition.
- Results are compiled and investigated PQ disturbances associated with solar energy and wind energy penetration into the utility grid are suggested.
- Finally, the effect of high solar energy and wind energy penetration levels on the power quality has been investigated based on the proposed power quality index. The results have been obtained for the wind energy, solar energy and simultaneous penetration of wind and solar energy.

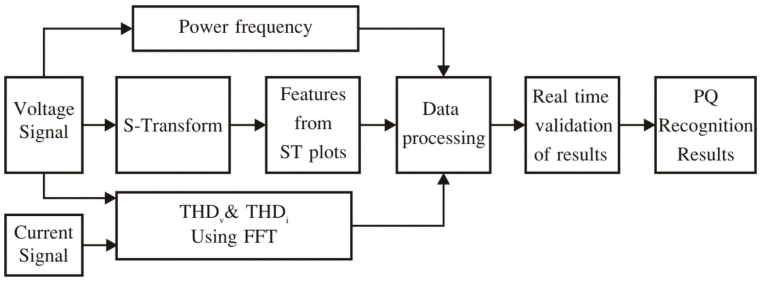

Figure 5.6 : Block scheme of PQ recognition

Power quality index is detailed in the section 4.2.1. Higher values of PQI indicate that quality of the power supplied is deteriorated adversely. Thus, values of this index are related to the quality of supply with low values for good quality of supply and higher values for poor quality of supply. Here, also the values of $\alpha, \beta, \gamma, \delta$, and σ are selected as unity.

5.5 RECOGNITION OF POWER QUALITY DISTURBANCES WITH WIND ENERGY: CASE STUDIES

This section details the detection of PQ disturbances associated with outage of the wind generator, grid synchronization of the wind generator, islanding of the test system from utility grid in the presence of diesel generator and wind speed variations. Voltage signal is decomposed using *S*-transform and *S*-matrix is obtained. PQ disturbances are investigated using the *S*-contour (time-frequency contour), amplitude curve, sum absolute values curve, phase and frequency contents of the signal. These curves are compared with the ST plots of standard PQ disturbances reported in chapter 3 for accurate detection of the available PQ disturbances. Proposed power quality index, total harmonic distortions of voltage and current injected by wind generators into the grid and maximum deviations of power frequency are used to investigate the effects of different wind energy penetration levels on the power quality. Results in the following subsections are provided with one wind generator connected on bus 650 with the help of CB2. Results with high wind energy penetration are obtained with two wind generators connected on the buses 680 and 646.

5.5.1 Grid Synchronization of Wind Generator

The wind generator of capacity 1.5 MW has been synchronized to the utility grid at 0.33 second and corresponding *S*-transform based plots are shown in Fig. 5.7. It can be observed that PQ transients exist for a period of 3 s. Voltage fluctuations, sag and swell can be observed from the amplitude curve in Fig. 5.7 (b). At the time of synchronization of wind generator, voltage sag is created due to inrush current drawn from the grid by wind generator. This reverses the power flow towards the wind generator due to which a voltage swell is created which ultimately leads to voltage fluctuations. These voltage fluctuations are source of the flicker. The voltage sag and swell are also observed in the sum absolute values curve in Fig. 5.7 (c). An isolated contour in Fig. 5.7 (a) indicates the presence of oscillatory transient (OT). Abrupt changes in the phase curve of Fig. 5.7 (d), also indicates the presence of transients at the time of synchronization of the wind generator. Finite values between the normalized frequencies 0.08 to 0.3 in the amplitude-frequency curve of Fig. 5.7 (e) indicate the presence of harmonics of various frequencies. Voltage in the system also increases approximately by 0.02 pu with the synchronization of wind generator due to injection of real power. It has also been observed that magnitude of detected PQ disturbances increases with wind energy penetration level of 3 MW as compared to 1.5 MW. Due to page limitations, the *S*-transform based plots have been plotted only for wind power penetration of 3 MW.

Power frequency during the event of grid synchronization of wind generator is shown in Fig. 5.8. Frequency variations for a period of 3.5 second are observed following the grid synchronization. Frequency varies between $60.5Hz$ and $59.7Hz$ with wind energy penetration of $3MW$ whereas frequency varies between $60.2Hz$ and $59.9Hz$ with wind generator of capacity $1.5MW$. Thus, the frequency deviations increase with the wind energy penetration level. High wind energy penetration degrade the frequency quality greatly. The THD_v and THD_i with wind energy penetrations of capacities $1.5MW$ and $3MW$ during the transient period are provided in Table 5.5, from which it can be established that the harmonics distortion level in the utility grid increases with the wind energy penetration level.

5.5.2 Outage of Wind Generator

Outage of the wind generator is simulated at 0.33 second. Active power supplied by wind generator to the utility grid decreases suddenly to zero during the outage event. This sudden change in power creates PQ disturbances in the utility grid. The *S*-transform based plots for voltage signal in phase-A during outage of wind generator are shown in Fig. 5.9. The sharp magnitude peak available in sum absolute values curve of Fig. 5.9 (c) indicates the presence of impulsive transient (IT). Abrupt change observed in the phase curve of Fig. 5.9 (d) also indicates the presence of impulsive transient component. A low magnitude change observed in the *S*-contour of Fig. 5.9

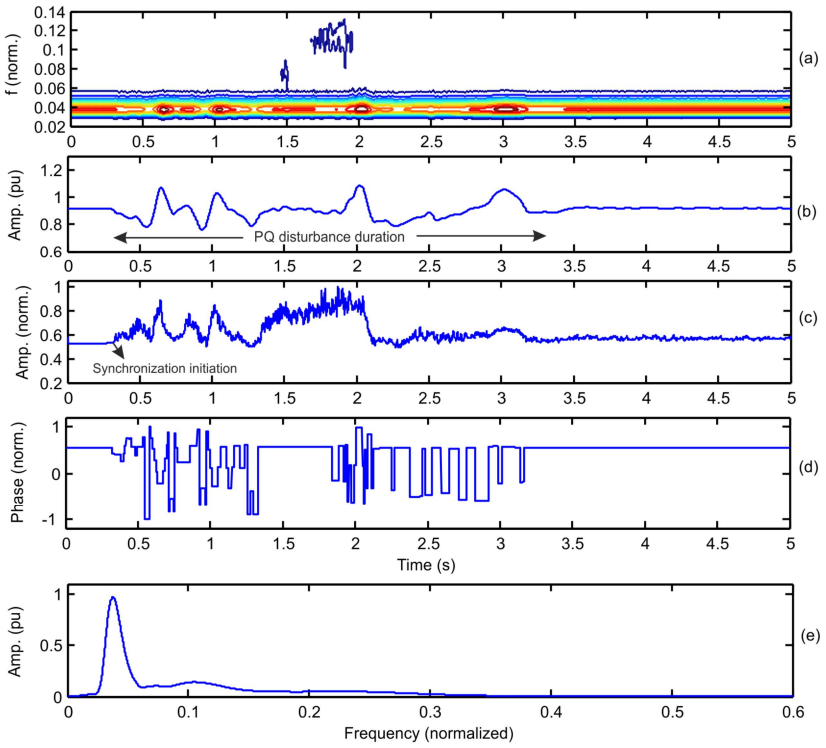

Figure 5.7 : (a) Frequency contour (b) Amplitude curve (c) Sum of absolute values curve (d) Phase curve (e) Amplitude-frequency curve from S-transform for grid synchronization of wind generator

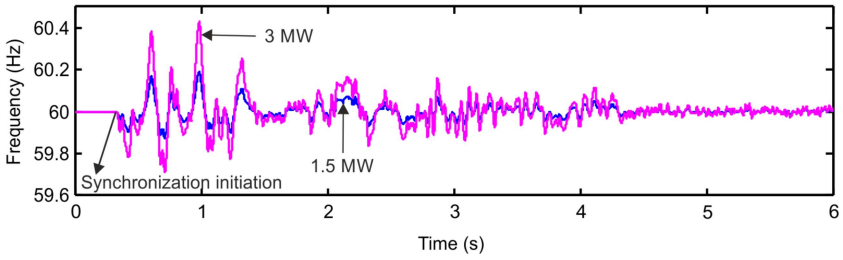

Figure 5.8 : Frequency variations during grid synchronization of wind generators

Table 5.5 : Total Harmonic Distortions of Voltage and Current with Wind Energy Penetration

S.No.	Different cases of study	THD_v (%)		THD_i (%)	
		$1.5MW$	$3MW$	$1.5MW$	$3MW$
1	Grid synchronization of wind generator	0.06	0.67	11.71	24.04
2	Outage of wind generator	1.15	7.61	16.03	19.54
3	Islanding	3.50	8.68	18.94	28.11
4	Wind speed variations	1.03	2.79	15.79	24.12

(a) at 0.33 s also indicates the presence of impulsive transient. Low magnitude ripples observed in the sum absolute values curve of Fig. 5.9 (c) following the outage event for a short duration. Finite values between the normalized frequencies 0.1 to 0.22 in frequency-amplitude curve of Fig. 5.9 (e) indicate the presence of harmonics. Voltage magnitude slightly increases after the outage by a value of 0.02 pu due to reduction in reactive power demand due to outage of induction generator.

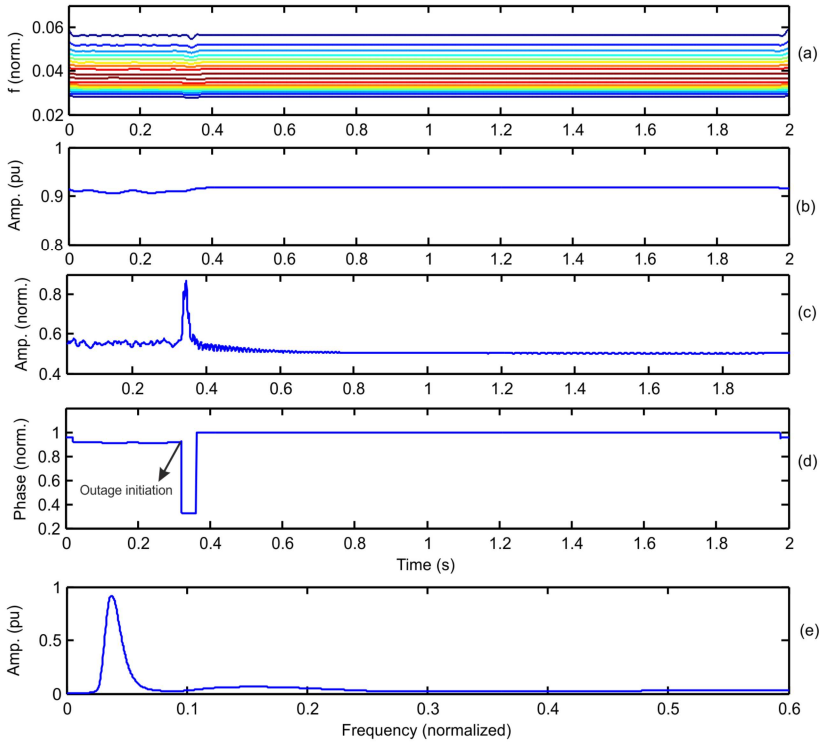

Figure 5.9 : (a) Frequency contour (b) Amplitude curve (c) Sum of absolute values curve (d) Phase curve (e) Amplitude-frequency curve from S-transform for outage of wind generator

Power frequency signal during outage of wind generators is shown in Fig. 5.10. Frequency drops suddenly to $59.95Hz$ and $59.82Hz$ following the outage of wind generators of capacities $1.5MW$ and $3MW$ respectively. Frequency is restored after a duration of 0.05 s. Due to high penetration level of wind energy, small variations in magnitude of the frequency are observed at the time of restoring of original value of frequency. The values of THD_v and THD_i with outage of wind generation of capacities 1.5 MW and 3 MW are provided in Table 5.5. High wind energy penetration increases the frequency deviations as well as THD_v and THD_i with outage of wind generators.

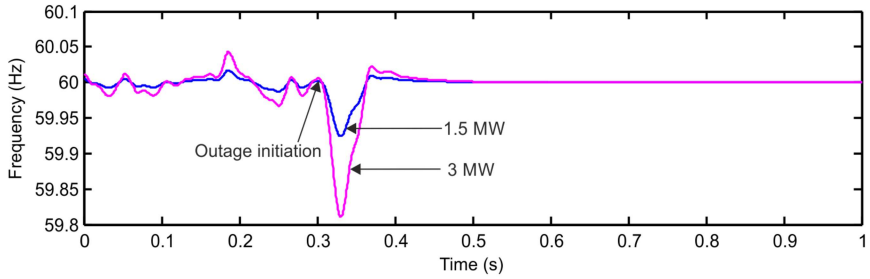

Figure 5.10 : Frequency variations during outage of wind generators

5.5.3 Islanding

Islanding of test system from the utility grid in the presence of $3MW$ wind generation is simulated at 0.33 s. Diesel generator is automatically switched on at the time of islanding. The test network is operated as mircogrid. Diesel generator supplies the reactive power drawn by the DFIG. The wind and diesel generators supply active power to the loads. Voltage fluctuations, sag and swell can be observed in the amplitude and sum absolute values curves of Fig. 5.11 (b) and (c) respectively. Variations in the voltage persists for a duration of 2.2 s. These voltage variations produce the flicker. Finite values between normalized frequencies 0.08 to 0.25 in the frequency-amplitude curve of Fig. 5.11 (e) detects the presence of harmonics. Isolated upper contours available in the *S*-contour of Fig. 5.11 (a) indicates the presence of oscillatory transients. Large variations in the phase curve of Fig. 5.11 (d) also indicates the presence of oscillatory transient. A transient over voltage followed by islanding operation has to be handled properly in the microgrid operation.

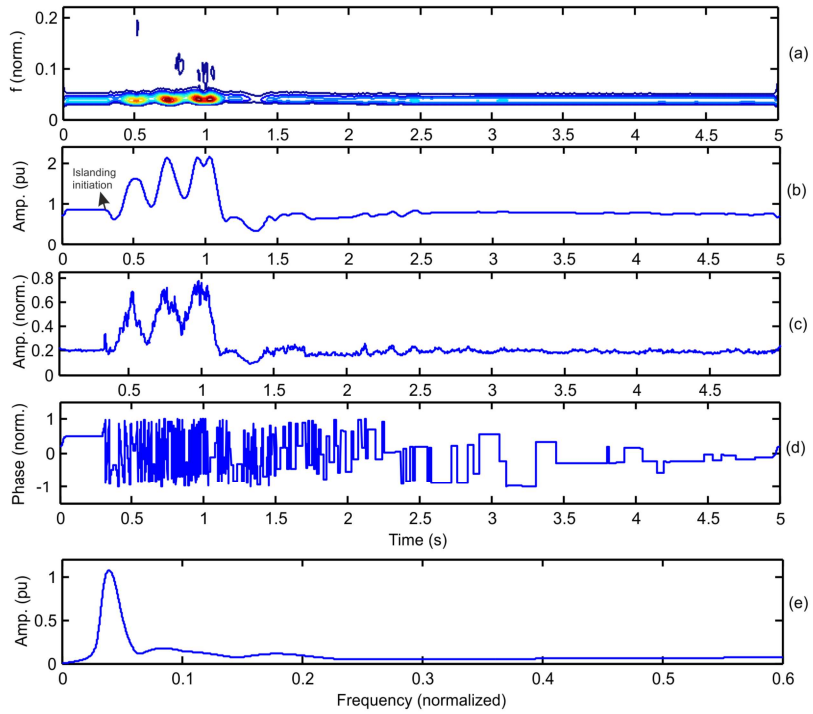

Figure 5.11 : (a) Frequency contour (b) Amplitude curve (c) Sum of absolute values curve (d) Phase curve (e) Amplitude-frequency curve from S-transform for islanding of test grid with diesel and wind generators

Frequency variations during the islanding event are shown in Fig. 5.12. With one wind generator of capacity $1.5MW$ integrated to the test network, the frequency first increases to $65Hz$ and later starts decreasing continuously since the generation is less than the demand. Power system network becomes unstable due to difference between the load demand and power supplied which ultimately lead to shut down of microgrid operation. With the 3 MW of wind energy generation, the frequency first increases to a value of $64Hz$ and finally reaches to a value of $60Hz$ resulting in stable operation as microgrid. This is due to the fact that the generation capacity matches with the load demand. The values of THD_v and THD_i during islanding event with wind energy penetration levels of 1.5 MW and 3 MW are provided in Table 5.5, from which it can be established that the harmonic distortion level in the utility grid increases with the wind energy penetration level.

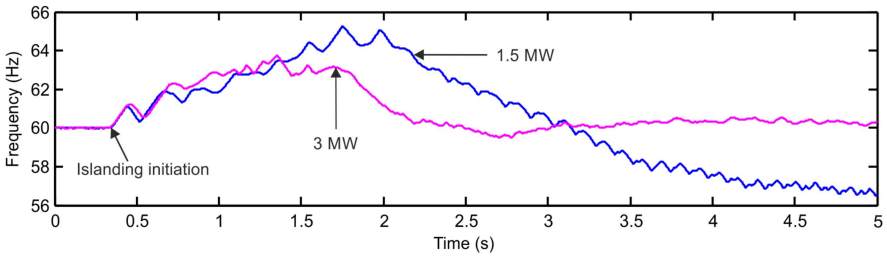

Figure 5.12 : Frequency variations during islanding event

5.5.4 Wind Speed Variations

The simulated wind speed variations for a period of 2 second are shown in Fig. 5.13. Abrupt changes in wind speed are simulated to investigate the maximum effect of wind speed variations on the quality of power.

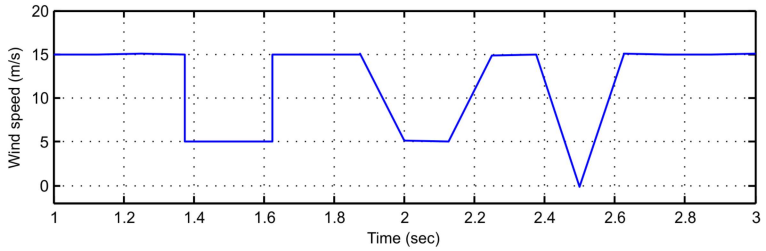

Figure 5.13 : Wind speed variations

The *S*-transform based plots of voltage signal with wind speed variations are shown in Fig. 5.14. The wind speed variations are transmitted as fluctuations in the mechanical torque input to the generator. This results in voltage fluctuations in the utility grid which can be observed in the amplitude curve of Fig. 5.14 (b). These voltage fluctuations produce a low magnitude flicker. The non-zero values between 0.08 and 0.25 normalized frequencies in the frequency-amplitude curve of Fig. 5.14 (e) indicate the presence of harmonics. Variations available in the phase curve of Fig. 5.14 (d) indicates the presence of low magnitude transients.

Frequency during wind speed variations are shown in Fig. 5.15. Variations of small magnitude between the frequencies $59.98Hz$ and $60.02Hz$ are observed due to wind speed variations in the presence of wind generator of capacity $1.5MW$. However, frequency varies between $59.96Hz$ and $60.04Hz$ in the presence of wind energy generation of capacity $3MW$. Hence, it has been observed that power frequency is not affected significantly even due to drastic change in the wind speed. The values of THD_v and THD_i with the variations in wind speed are provided in Table 5.5, from which it can be established that the wind energy penetration level increases the values of THD_v and THD_i. It is also established that frequency deviations also increase with the wind energy penetration level.

Maximum power frequency deviations from standard value of $60Hz$ with wind generation of capacities $1.5MW$ and $3MW$ during all the events of study are provided in Table 5.6. It has been observed that maximum frequency deviations are detected with the islanding event followed by the synchronization, outage and wind speed variations. Frequency deviations increase with increase in the penetration level of wind energy.

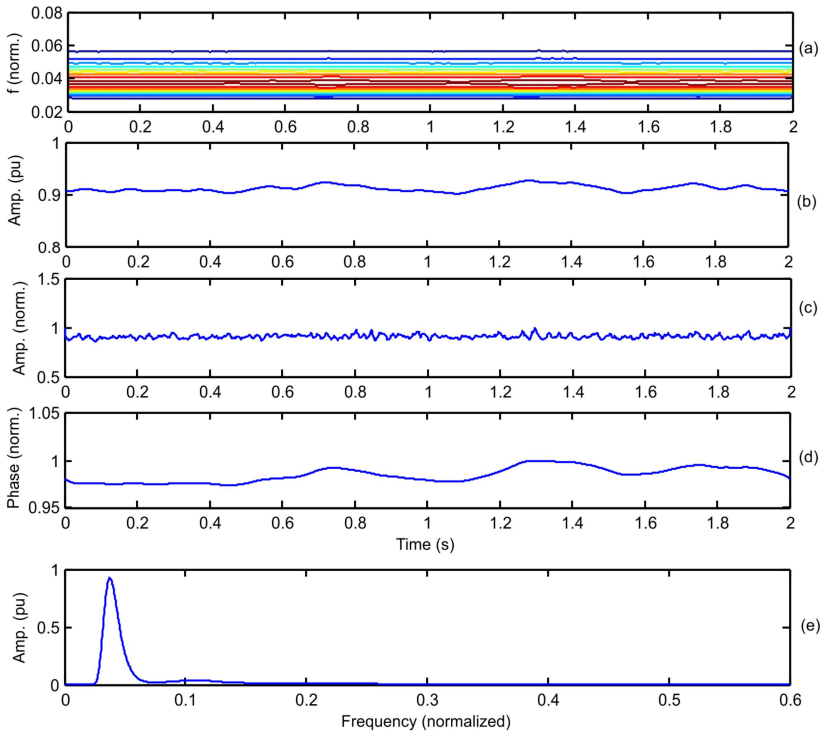

Figure 5.14 : (a) Frequency contour (b) Amplitude curve (c) Sum of absolute values curve (d) Phase curve (e) Amplitude-frequency curve from S-transform for wind speed variations

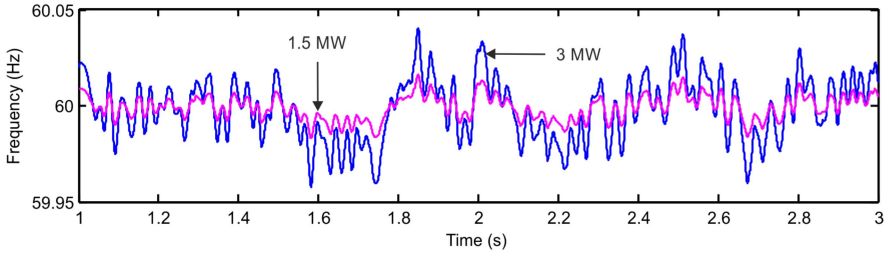

Figure 5.15 : Frequency variations during wind speed variations

The power quality indexes for the events with wind generators of capacities $1.5MW$ and $3MW$ are presented in the Table 5.6. It has been observed that overall power quality is adversely affected in case of islanding followed by synchronization, wind speed variations, and outage. It is further observed that the power quality deteriorated with the level of wind energy penetration.

5.6 RECOGNITION OF POWER QUALITY DISTURBANCES WITH SOLAR ENERGY PENETRATION: CASE STUDIES

This section details the simulation results related to the detection of PQ disturbances associated with grid synchronization and outage of solar PV system. PQ events associated with sudden change in solar insolation have also been investigated. Voltage signals for various events has been decomposed using *S*-transform and *S*-matrix is obtained. PQ events are investigated utilizing the

Table 5.6 : Maximum Frequency Deviations and Power Quality Index with Wind Energy Penetration

S.No.	Event description	Frequency deviation (Hz)		Power quality index	
		$1.5MW$	$3MW$	$1.5MW$	$3MW$
1	Grid synchronization of wind generator	0.200	0.500	19.052	57.684
2	Outage of wind generator	0.050	0.180	4.125	9.728
3	Islanding	3.105	4.080	517.28	357.576
4	Wind speed variations	0.020	0.038	8.519	12.642

various S-transform based plots. The proposed power quality index, THD_v, THD_i and maximum frequency deviations are used to investigate the impacts of different solar PV energy penetration levels on the power quality. Investigation of PQ disturbances with grid integration of solar PV system during various operational events is detailed in the following subsections.

5.6.1 Grid Synchronization of Solar PV Plant

The solar PV system is synchronised with the test system at 0.1 s. Various plots based on S-transform for voltage waveform of phase-A are shown in Fig. 5.16. It can be observed that PQ disturbances exist for a period of 0.35 s. Voltage unbalance with sag and swell has been observed in the amplitude curve of Fig. 5.16 (c). Voltage first decreases as the power starts flowing from the solar PV system to the feeder in a direction opposite to the direction of conventional power flow. After this, voltage starts increasing and creates a low magnitude voltage swell. After a period of 0.35 s, voltage fluctuations die out. Voltage in the test feeder is slightly higher as compared to the voltage without solar PV energy penetration. Observed voltage sag is caused by the inrush current produced due to small inevitable difference between voltages of solar PV plant and grid. Duration and severity of produced inrush current depends on the system impedance, nonlinear magnetic saturation characteristic, magnitude and sign of flux linkage of the coupling transformer. Presence of PQ disturbances has also been verified by the high magnitude with variations available in sum absolute values curve of Fig. 5.16 (d). High frequency contour available in S-contour of Fig. 5.16 (b) and second frequency component available in Fig. 5.16 (f) indicates the presence of flicker. Change in the phase curve shown in Fig. 5.16 (e), also indicates the presence of low magnitude transients in the grid at PCC. From Fig. 5.16 (c), it is also depicted that voltage after synchronization of solar PV system increases slightly by 0.01 pu and it provides voltage support in the low voltage networks. However, if the penetration level is high, over voltage in the feeder might result. It has also been observed that the magnitude of detected PQ disturbances increases with the solar PV generators of capacities of $500kW$ and $1MW$. However, due to page limitations, the S-transform based plots have not been plotted for these generators.

Frequency variations during the event of grid synchronization of solar PV system is shown in Fig. 5.17. Frequency drops suddenly to $59.6Hz$, $59.20Hz$, and $57.9Hz$ following the grid synchronization of solar PV generators of capacities $100kW$, $500kW$ and $1MW$ respectively. The standard frequency of $60Hz$ is restored within a period of 0.35 s. Low magnitude oscillations are observed during this period. High penetration level degrades quality of the frequency greatly. The THD_v and THD_i with solar PV energy generators of capacities $100kW$, $500kW$ and $1MW$ during the transient period are provided in Table 5.7, from which it can be observed that harmonic distortions level in the power network increases with increase in the penetration level. It is also observed that the values of THD in voltage and current are reduced below 5 % within a duration of 0.35 s after the event occurrence which is in accordance with IEEE-519 standard.

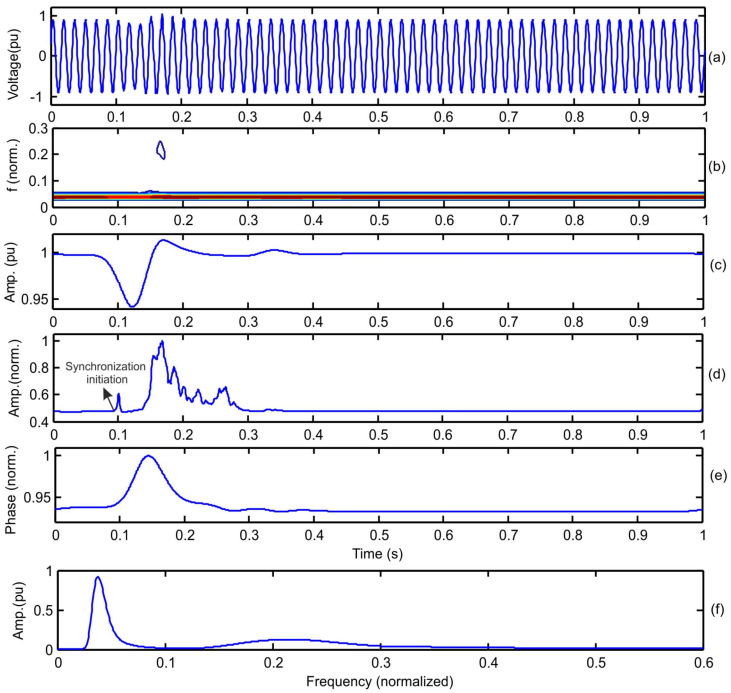

Figure 5.16 : (a) Voltage signal at PCC (b) Frequency contour (c) Amplitude curve (d) Sum of absolute values curve (e) Phase curve (f) Amplitude-frequency curve from S-transform for grid synchronization of solar PV system

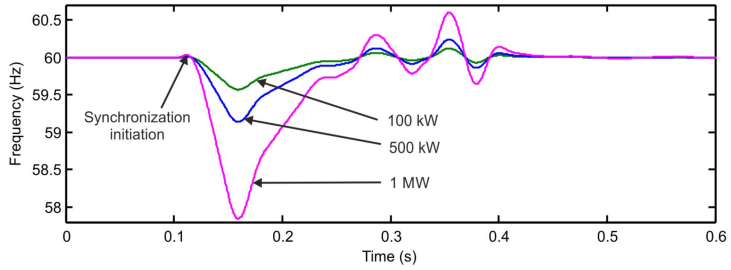

Figure 5.17 : Frequency variations during grid synchronization of solar PV system

Table 5.7 : Total Harmonic Distortions of Voltage and Current with Solar Energy Penetration

S.No.	Different cases of study	Class symbol	THD_v (%)			THD_i (%)		
			$100kW$	$500kW$	$1MW$	$100kW$	$500kW$	$1MW$
1	Grid synchronization of solar PV system	CS1	1.50	2.56	5.93	12.06	93.03	163.71
2	Outage of solar PV system	CS2	3.07	5.21	8.23	16.36	76.03	150.03
3	Change in solar insolation	CS3	5.83	6.58	7.57	21.68	56.79	80.41

5.6.2 Outage of Solar PV Plant

The outage of solar PV plant has been simulated at the end of 18^{th} cycle from start of the simulation. Active power supplied to the grid during outage of the solar PV plant decreases suddenly to zero. This sudden change in power creates PQ disturbances in the utility grid. The *S*-transform based plots for voltage signal of phase-A during outage of solar PV plant are shown in Fig. 5.18. It has been observed from the amplitude curve of Fig. 5.18 (c), that voltage in the feeder decreases by a value of 0.002 pu. This is expected as power needed at the load point will be supplied from the utility grid and maximum voltage drop in the feeder will be observed. The outage of solar PV generator has been detected by high peak available in the sum absolute values curve of Fig. 5.18 (d). This high peak also indicates the presence of impulsive transient (IT). The phase obtained from *S*-transform shown in Fig. 5.18 (e) also changes and it increases by a small amount. From the Fig. 5.18 (f), it can be observed that there is no high frequency component available with significantly high magnitude. High frequency transients and flicker have not been detected with the outage of solar PV system.

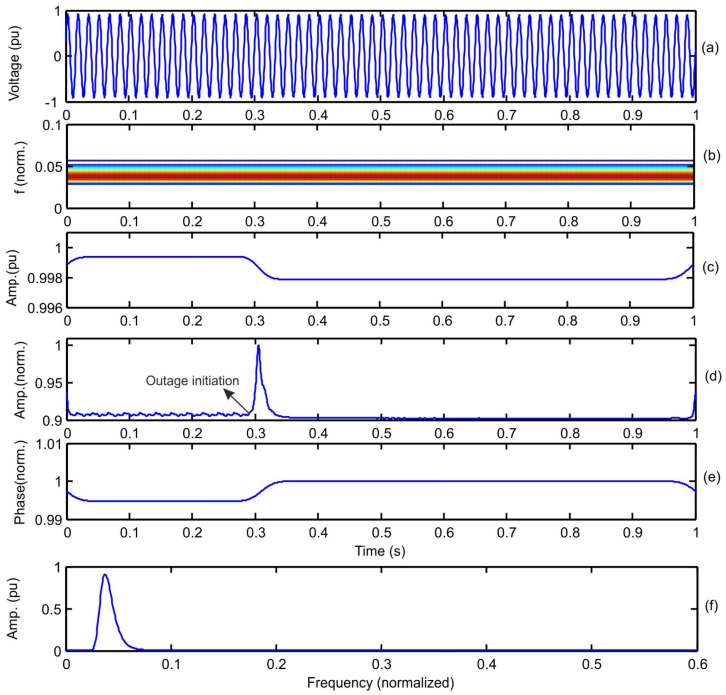

Figure 5.18 : (a) Voltage signal at PCC (b) Frequency contour (c) Amplitude curve (d) Sum of absolute values curve (e) Phase curve (f) Amplitude-frequency curve from *S*-transform for outage of solar PV system

Frequency signals during outage of solar PV generators are shown in Fig. 5.19. Frequency drops suddenly to $59.954Hz$, $59.84Hz$, and $59.81Hz$ due to outage of solar PV generators of capacities $100kW$, $500kW$ and $1MW$ respectively. Frequency is restored after a duration of 0.05 s. Due to high penetration level, small magnitude variations in the frequency are observed while restoring the standard value of frequency. These variations are acceptable by most of the grid codes in the world. The THD_v and THD_i with outage of solar PV generators of capacities $100kW$, $500kW$ and $1MW$ are provided in Table 5.7. High penetration level increases the magnitude of frequency deviations as well as THD_v and THD_i.

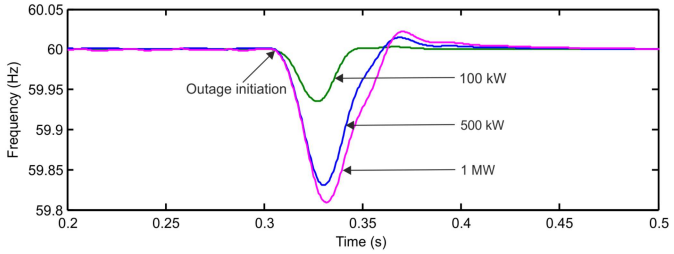

Figure 5.19 : Frequency variations during outage of solar PV system

5.6.3 Sudden Change in Solar Insolation

The solar insolation abruptly changes from $1000w/m^2$ to $600w/m^2$ at 18^{th} cycle. Plots based on the *S*-transform are shown in Fig. 5.20. It can be observed from Fig. 5.20 (c) that voltage drops with decrease in the solar insolation creating a voltage sag. Voltage fluctuations are also observed by continuous variations in the voltage magnitude. These voltage variations have also been observed in the sum absolute values curve of Fig. 5.20 (d), by the peaks available in the curve. These also indicates the presence of low magnitude flicker in the voltage. Low magnitude transients have also been observed on surface of the *S*-contour of Fig. 5.20 (b). Phase also increases by an amount of 0.0035 (normalized), and variations in the phase have also been observed.

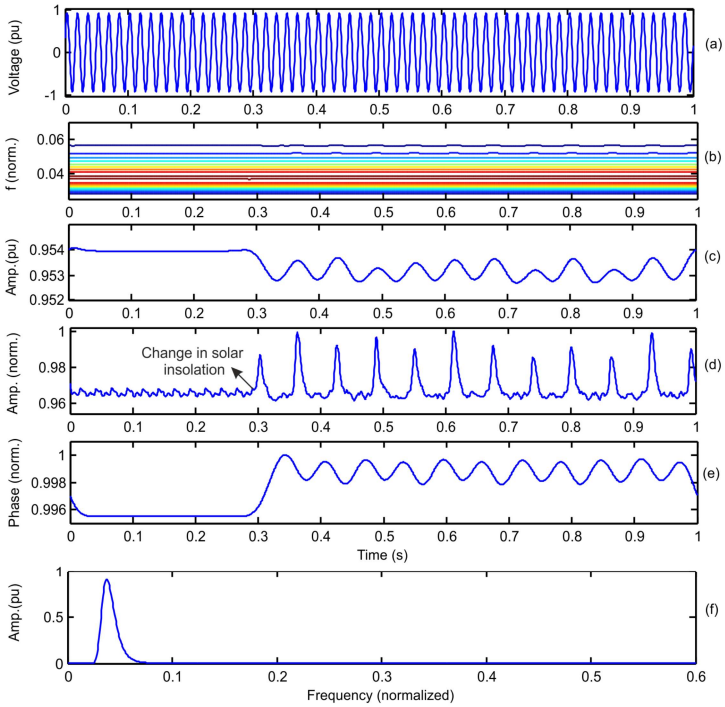

Figure 5.20 : (a) Voltage signal at PCC (b) Frequency contour (c) Amplitude curve (d) Sum of absolute values curve (e) Phase curve (f) Amplitude-frequency curve from *S*-transform for abrupt change in solar insolation

Frequency variations with abrupt change in solar insolation are provided in Fig. 5.21. Due to sudden change in the solar insolation, continuous variations in the power frequency with small magnitude of $0.08Hz$, $0.18Hz$ and $0.35Hz$ have been observed with solar PV generators of capacities $100kW$, $500kW$ and $1MW$ respectively. These variations are accepted by most of the grid codes

adopted by different countries in the world. The THD_v and THD_i with sudden change in solar insolation with solar PV generators of capacities $100kW$, $500kW$ and $1MW$ are provided in Table 5.7.

Maximum power frequency variations with penetration of $100kW$, $500kW$ and $1MW$ into the utility grid during all the events of study are provided in Table 5.8. It has been observed that maximum frequency deviations are observed with grid synchronization of solar PV following the change in solar insolation and minimum with outage of solar PV generator. Frequency deviations increase with increase in the penetration level of solar PV energy. Solar energy penetration level with the solar PV system of capacity $1MW$ is 29%. This high penetration level of solar energy has deviated the frequency by 2.1 Hz. If this deviation in frequency is not allowed by the grid codes then it may cause technical challenges such as protection, stability etc. If this deviation trigger the protection then the solar PV generator may not be integrated to the utility grid. It is observed that penetration level increases the magnitude of frequency deviations as well as THD_v and THD_i. However, maximum increase in THD_i has been observed with the grid synchronization following the outage and change in solar insolation. The change in THD_v is maximum with outage following the change in solar insolation and synchronization.

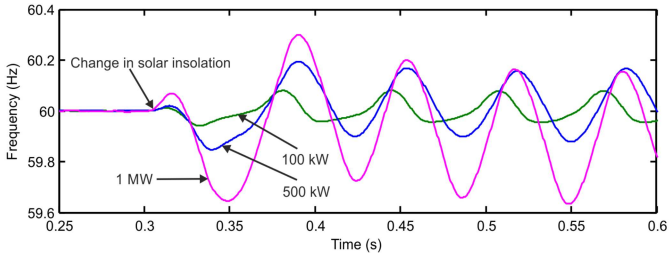

Figure 5.21 : Frequency variations during abrupt change in solar insolation

Table 5.8 : Maximum Power Frequency Deviations with Solar PV Energy Penetration

S.No.	Different cases of study	Frequency deviations (Hz)		
		$100kW$	$500kW$	$1MW$
1	Grid synchronization of solar PV system	0.430	0.80	2.10
2	Outage of solar PV system	0.046	0.16	0.19
3	Change in solar insolation	0.080	0.18	0.35

Power quality indices for the events under investigation with solar PV generators of capacities $100kW$, $500kW$, and $1MW$ are provided in Table 5.9. All weights $\alpha, \beta, \gamma, \delta$ and σ have been selected unity for present study. It has been observed that with increase in the solar PV penetration level in the grid, the power quality is adversely affected. Overall maximum effect on the PQ is observed with the grid synchronization of solar PV system followed by change in the solar insolation and minimum with outage of the solar PV system.

5.7 RECOGNITION OF POWER QUALITY DISTURBANCES IN HYBRID POWER SYSTEM: CASE STUDIES

This section presents the analysis of PQ disturbances associated with various events in the hybrid power system interfaced with wind and solar energy systems. Study of the PQ disturbances in the hybrid power system has been carried out without integrating the diesel generator to the test network. The *S*-transform based plots for the voltage signal during the events under investigation have been compared with respective plots of standard PQ disturbances presented in chapter 3 to

Table 5.9 : Power Quality Index with Solar Energy Penetration

S.No.	Different cases of study	Power quality index		
		$100kW$	$500kW$	$1MW$
1	Grid synchronization of solar PV system	9.642	32.558	68.228
2	Outage of solar PV system	4.034	16.612	32.352
3	Change in solar insolation	7.231	28.256	36.731

effectively detect the PQ disturbances. All the events have been simulated at 0.33 s. Proposed power quality index, THD_v, THD_i and maximum frequency deviations are used to rate the various operational events in terms of power quality.

5.7.1 Islanding in the Presence of Wind Power Generation

Islanding of the test system with wind power generation is performed at 0.33 s by opening the IID switch. The *S*-transform based plots for voltage waveform are shown in Fig. 5.22. Voltage fluctuations, sag and swell are observed from the amplitude curve of Fig. 5.22 (c). Fluctuations in the voltage can also be observed from sum absolute values curve of Fig. 5.22 (d). The results are plotted for 1 s. However, it has been observed that voltage fluctuations persist continuously due to gap between the load demand and generated power. Further, the source of reactive power is also not available for the DFIG wind generator. Presence of low magnitude impulsive transient (IT) is detected by high magnitude peak available in sum absolute values curve and frequency contour. Abrupt changes in phase plot of Fig. 5.22 (e) also validate the presence of impulsive transient component. Finite values through out normalized frequency range in the frequency-amplitude plot beyond the peak of fundamental frequency as shown in Fig. 5.22 (f) indicate the presence of IT. Frequency variations during islanding event with the presence of wind generation are illustrated in Fig. 5.23. It is observed that frequency rises to a value of 68 Hz (approx.) and then becomes constant.

5.7.2 Islanding in the Presence of Solar PV Power Generation

Islanding in the presence of solar PV system is performed at 0.33 s and respective plots based on *S*-transform of voltage signal are illustrated in Fig. 5.24. A voltage sag is detected by decreased magnitude of amplitude plot illustrated in Fig. 5.24 (c). It is also observed from this curve that voltage continuously increases followed by the voltage sag. This trend of voltage is also validated by similar changes in sum absolute values plot of Fig. 5.24 (d). High magnitude peak available in sum absolute value curve of Fig. 5.24 (d) and a projected contour observed in the frequency contour of Fig. 5.24 (b) detects presence of the impulsive transient. Abrupt changes in the phase curve of Fig. 5.24 (e) also indicate the transient components. Finite values between normalized frequencies 0.06 to 0.25 as shown in amplitude-frequency plot of Fig. 5.24 (f) indicate the presence of harmonics. Frequency signals during islanding event in the presence of solar PV system are provided in Fig. 5.25. Frequency continuously rises to 68 Hz (approx.) and becomes constant at this value.

5.7.3 Islanding in the Presence of Wind Power and Solar PV Power Generations

The IID switch is turned off at 0.33 s to simulate the islanding in the presence of wind and solar PV generation. Fig. 5.26 illustrates the respective *S*-transform based plots of voltage signal. Voltage fluctuations with sags and swells are observed in the amplitude and sum absolute values plots illustrated respectively in Fig. 5.26 (c) and (d). Variations in magnitude of frequency contour illustrated in Fig. 5.26 (b) also indicate the presence of voltage fluctuations with sag and swell. Low

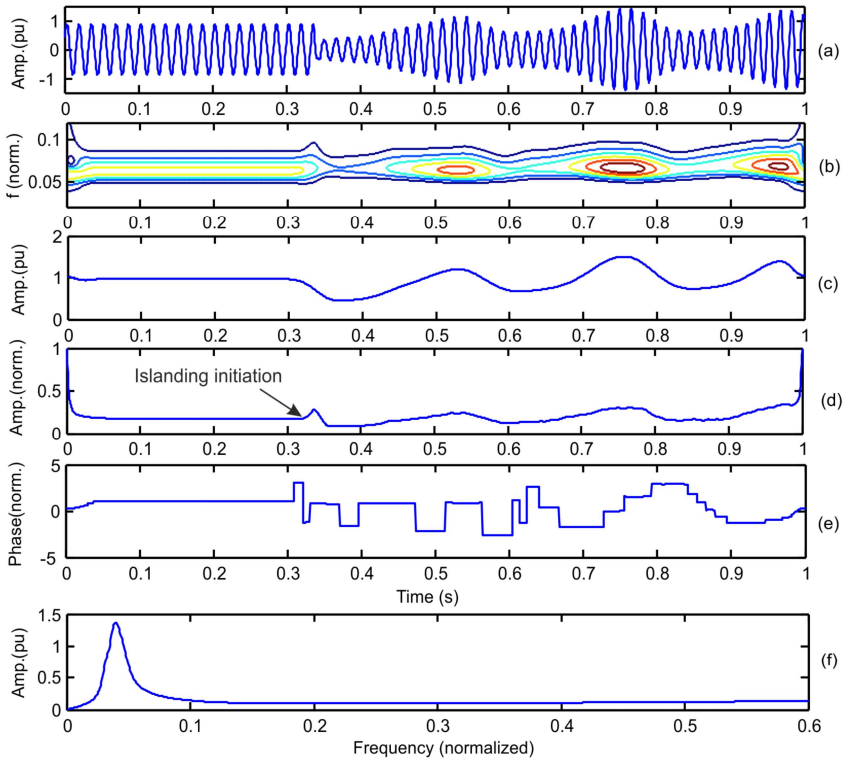

Figure 5.22 : (a) Voltage signal (b) *S*-contour (c) Amplitude curve (d) Sum of absolute values curve (e) Phase curve and (f) Amplitude-frequency curve from *S*-transform for islanding with wind generator

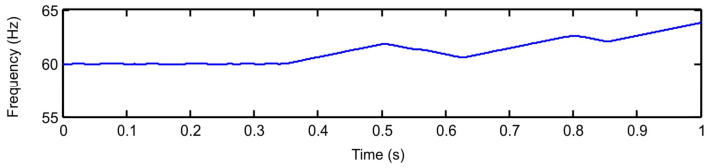

Figure 5.23 : Frequency variation during islanding with wind generator

magnitude peak available in sum absolute values plot at the time of islanding indicates presence of the IT. Presence of these transient components is also validated by abrupt changes in phase curve of Fig. 5.26 (e). Frequency variations during islanding event in the simultaneous presence of wind and solar PV power generations are shown in Fig. 5.27. Frequency continuously rises up to 64 Hz (approx.) and achieves constant value.

5.7.4 Outage of Wind Generator in the Presence of Solar PV system

The outage of wind generator with solar PV system is simulated at 0.33 s and respective *S*-transform based plots of voltage signal are depicted in Fig. 5.28. A sharp magnitude peak available in sum absolute values curve illustrated in Fig. 5.28 (d) detects the presence of impulsive transient. Change in phase plot of Fig. 5.28 (e) is also due to presence of IT. A voltage swell is observed in amplitude curve of Fig. 5.28 (c) by increase in the magnitude by an amount of 2%. This is due to reduced demand of reactive power with outage of DFIG based wind generator. Finite

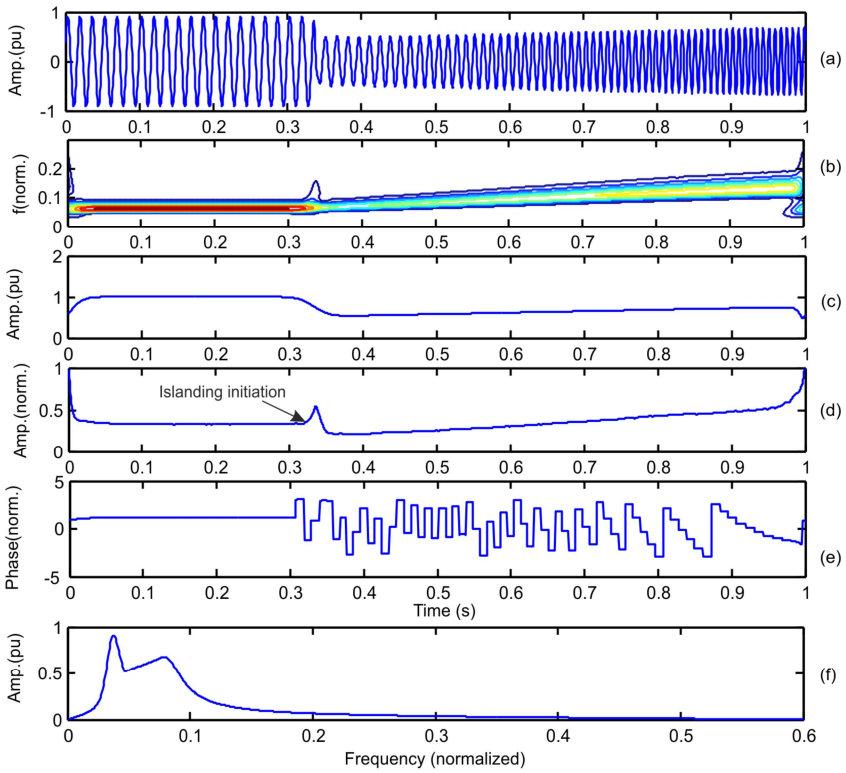

Figure 5.24 : (a) Voltage signal (b) *S*-contour (c) Amplitude curve (d) Sum of absolute values curve (e) Phase curve and (f) Amplitude-frequency curve from *S*-transform for islanding with solar PV system

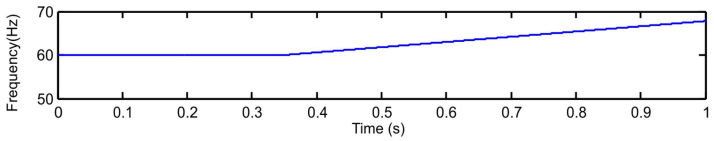

Figure 5.25 : Frequency variations during islanding with solar PV system

values between normalized frequencies 0.1 to 0.2 as shown in Fig. 5.28 (f) indicate presence of the harmonics. Power frequency variations during outage of wind generator with solar PV system is illustrated in Fig. 5.29. Frequency drops suddenly to 59.82 Hz and restores to original values after a short duration (<0.1 second).

5.7.5 Outage of Solar PV system in the Presence of Wind Power Generation

Outage of the solar PV system with wind power generation integrated to test system is simulated at 0.33 s. Respective plots based on *S*-transform are illustrated in Fig. 5.30. A sharp magnitude peak available in sum absolute values plot illustrated in Fig. 5.30 (d) indicates the presence of impulsive transient. Change in the phase curve of Fig. 5.30 (e) is also due to the presence of IT. A low magnitude voltage sag followed by voltage swell is observed in the amplitude plot shown in Fig. 5.30 (c). Finite values between normalized frequencies 0.1 to 0.25 of plot shown in Fig. 5.30 (f) detects the low magnitude harmonics. Power frequency signal during the outage event

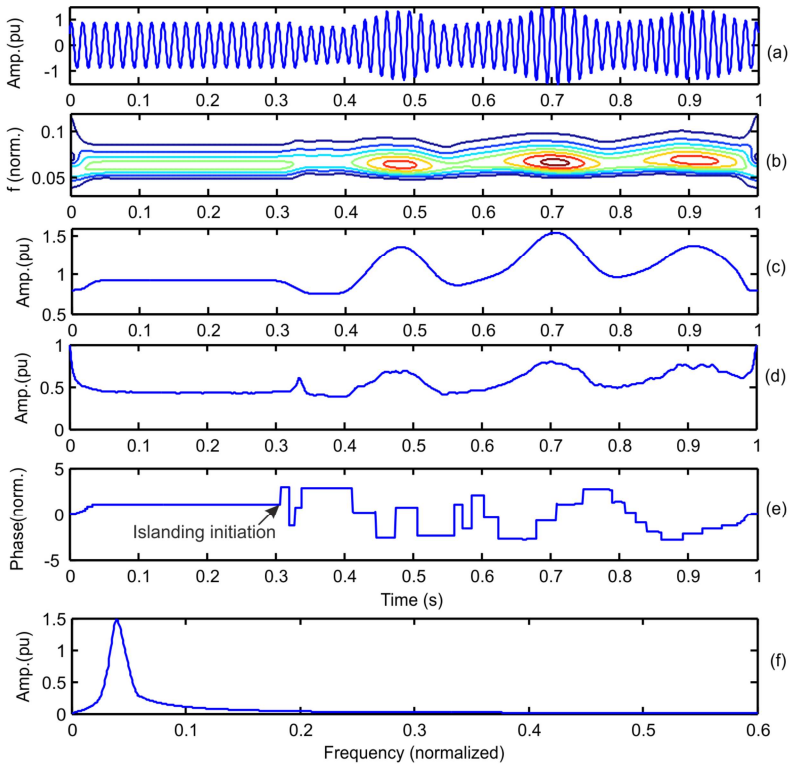

Figure 5.26 : (a) Voltage signal (b) *S*-contour (c) Amplitude curve (d) Sum of absolute values curve (e) Phase curve and (f) Amplitude-frequency curve from *S*-transform for islanding with wind and solar PV generations

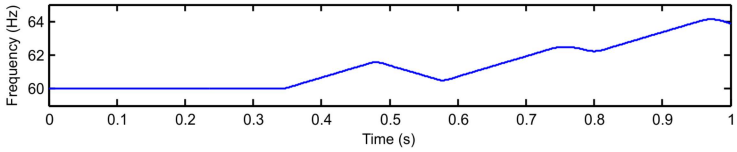

Figure 5.27 : Frequency variations during islanding with wind and solar PV generation

is provided in Fig. 5.31. Frequency suddenly drops to 59.95 Hz followed by the outage event and attains original value during a period of 0.05 s.

5.7.6 Simultaneous Outage of Solar PV System and Wind Generator

The outage of solar PV system and wind generator is simulated simultaneously at 0.33 s and respective *S*-transform based plots of voltage signal are illustrated in Fig. 5.32. Isolated contour observed in the frequency contour of Fig. 5.32 (b) detects the presence of low magnitude oscillatory transient (OT). A sharp magnitude peak available in sum absolute values curve illustrated in Fig. 5.32 (d) detects the IT. Significant change observed in phase curve of Fig. 5.32 (e) also detects OT and IT. Finite values between normalized frequencies 0.1 to 0.25 in plot of Fig. 5.32 (f) detects the presence of low magnitude harmonics. Variations of power frequency during outage event are shown in Fig. 5.33. Frequency suddenly drops to 59.82 Hz due to outage event and regains the original value during a time period of 0.06 s.

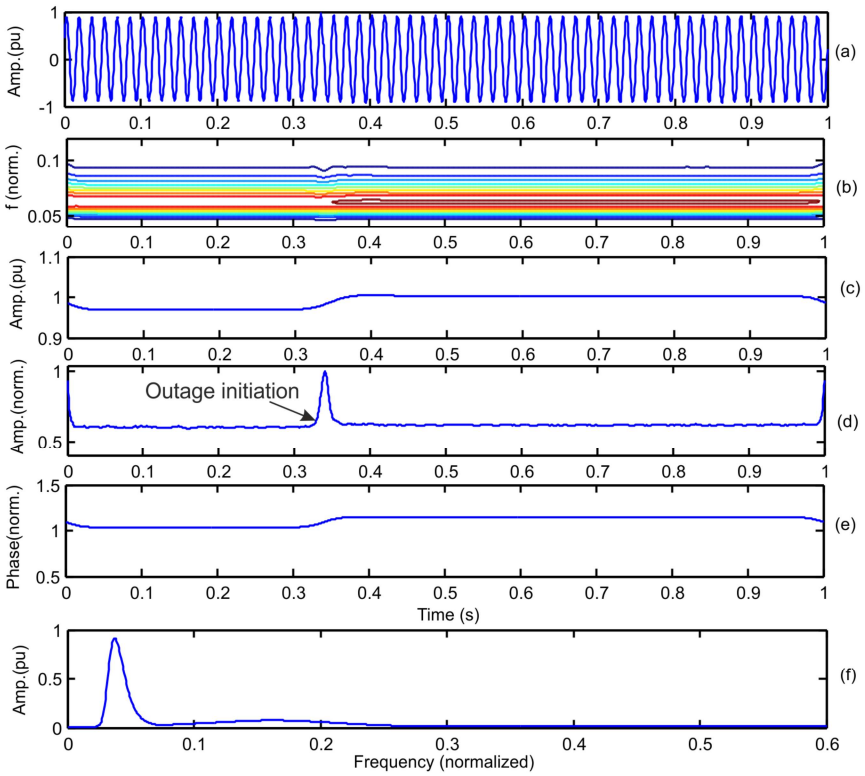

Figure 5.28 : (a) Voltage signal (b) *S*-contour (c) Amplitude curve (d) Sum of absolute values curve (e) Phase curve and (f) Amplitude-frequency curve from *S*-transform for outage of wind generator with solar PV generation

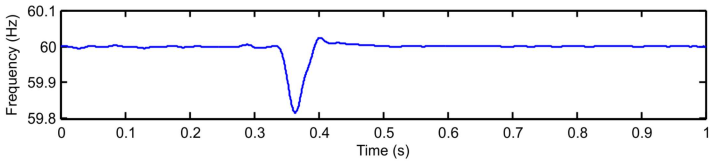

Figure 5.29 : Frequency variations during outage of wind generator with solar PV generation

5.7.7 Grid Synchronization of Wind Generator in the Presence of Solar PV System

Wind generator of the capacity 1.5 MW has been synchronized to utility grid with solar PV system at 0.33 s and corresponding *S*-transform based plots are illustrated in Fig. 5.34. Decrease in magnitude of amplitude curve between 0.33 s to 0.9 s as illustrated in Fig. 5.34 (c) detects the presence of voltage sag. This is due to the reactive power drawn by DFIG from utility grid at synchronization instant and reversal of power flow in the feeder. Sharp peak available in the sum absolute values curve of Fig. 5.34 (d) indicates the presence of IT. Change in the phase curve of Fig. 5.34 (e) between 0.33 to 0.5 s also detects the IT. Finite values between normalized frequencies 0.1 to 0.3 in the plot of Fig. 5.34 (f) detect the harmonics. Frequency signal during synchronization event is illustrated in Fig. 5.35. It is observed that the frequency variations appear between 0.33 s to 0.55 s. The original value of frequency is restored after two cycles of decrease in frequency followed by increase. Maximum frequency deviation of 0.18 Hz has been observed.

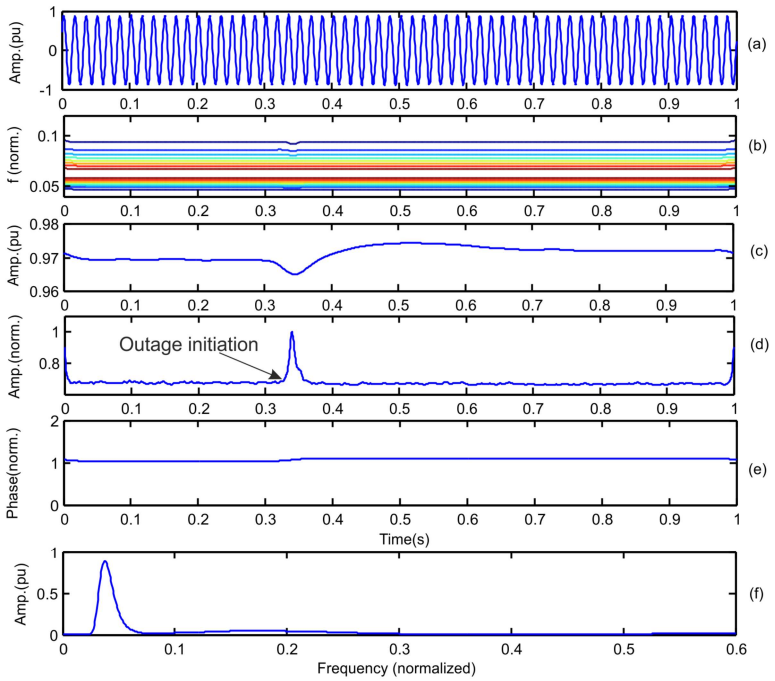

Figure 5.30 : (a) Voltage signal (b) *S*-contour (c) Amplitude curve (d) Sum of absolute values curve (e) Phase curve and (f) Amplitude-frequency curve from *S*-transform for outage of solar PV system with wind generation

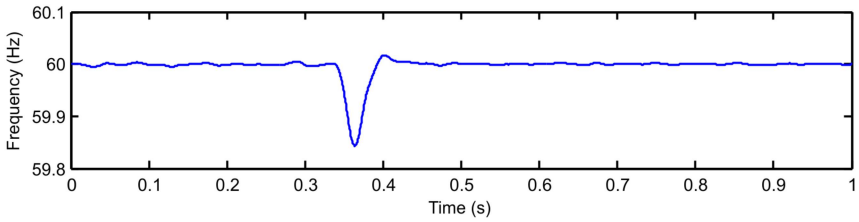

Figure 5.31 : Frequency variations during outage of solar PV system with wind power generation

5.7.8 Grid Synchronization of Solar PV System in the Presence of Wind Power Generation

A solar PV system of capacity 1 MW is synchronized to the utility grid at 0.33 s and respective *S*-transform based plots of voltage signal are provided in Fig. 5.36. Decreased magnitude of amplitude curve between 0.33 s to 0.7 s in Fig. 5.36 (c) indicates presence of the sag in voltage. This is detected due to change in rate of reactive power flow and power reversal in the feeder due to synchronization of solar PV generator. Sharp peak available in the sum absolute values curve of Fig. 5.36 (d) indicates the presence of IT. Change in the phase curve of Fig. 5.36 (e) is also an indication of IT. Finite values between normalized frequencies 0.15 to 0.35 in the plot of Fig. 5.36 (f) detect the harmonics. Presence of harmonics have also been indicated by ripples observed on the surface of sum absolute values plot of Fig. 5.36 (d). Harmonics are also observed on the surface of *S*-contour as shown in Fig. 5.36 (b). Power frequency signal is provided in the Fig. 5.37. Frequency oscillations are observed between 0.33 s to 0.58 s with maximum deviation of 0.06 Hz.

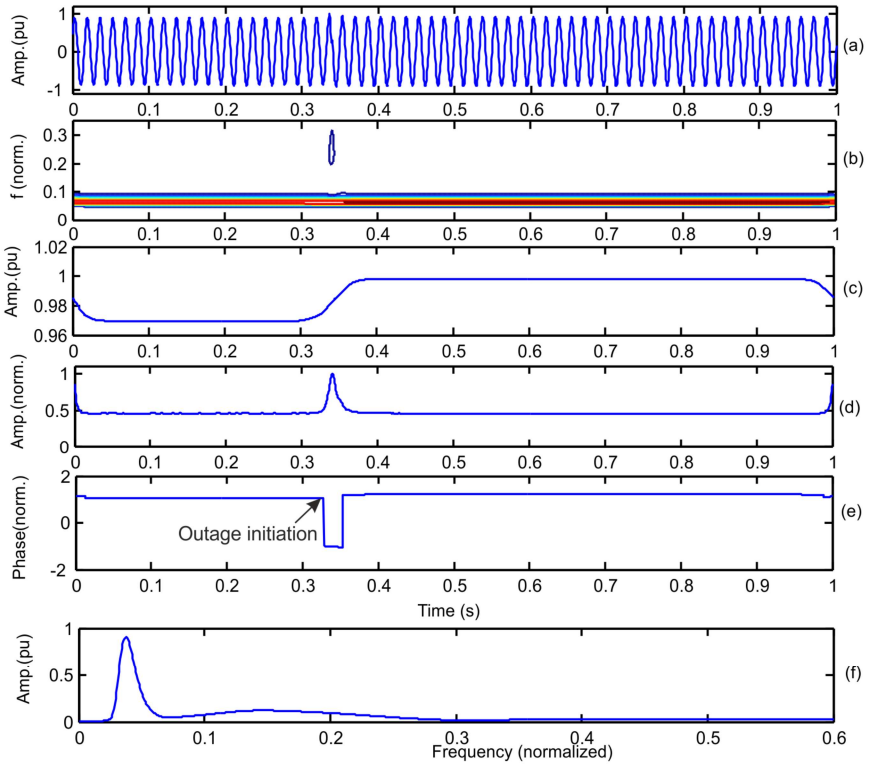

Figure 5.32 : (a) Voltage signal (b) *S*-contour (c) Amplitude curve (d) Sum of absolute values curve (e) Phase curve and (f) Amplitude-frequency curve from *S*-transform for simultaneous outage of wind and solar PV generators

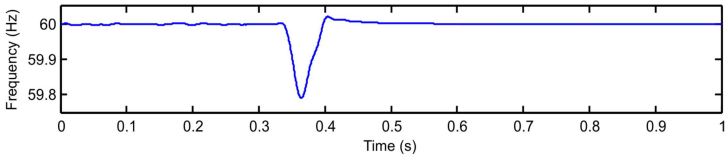

Figure 5.33 : Frequency variations with simultaneous outage of wind and solar PV generators

5.7.9 Simultaneous Grid Synchronization of Solar PV system and Wind Generator

Solar PV system and wind generator are simultaneously synchronized to the utility grid at 0.33 s and respective *S*-transform based plots of voltage signal are illustrated in Fig. 5.38. The voltage swell followed by a sag are observed as shown in amplitude curve of Fig. 5.38 (c). This is observed due to reactive power flow on PCC at the time of synchronization of RE sources. Isolated upper contour in the frequency contour of Fig. 5.38 (b) indicates presence of the oscillatory transient. High magnitude peak in the sum absolute values curve of Fig. 5.38 (d) at 0.33 s indicates presence of the IT. Continuous high magnitude in this curve is due to the high magnitude oscillatory transients and ripples on the surface of this curve are due to harmonics. Finite values in the frequency amplitude curve of Fig. 5.38 (f) between normalized frequencies 0.1 to 0.3 detect the harmonics. Abrupt changes in phase curve of Fig. 5.38 (e) also validates the presence of OT and IT. Power frequency signal during synchronization event is shown in Fig. 5.39. Original value of 60 Hz is attained following the oscillations between 0.33 s to 0.70 s with a maximum deviation of

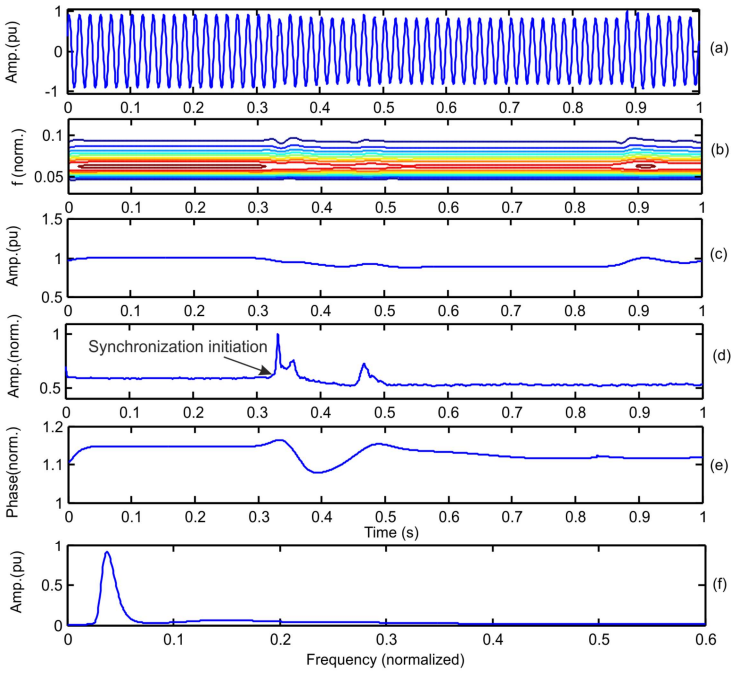

Figure 5.34 : (a) Voltage signal (b) S-contour (c) Amplitude curve (d) Sum of absolute values curve (e) Phase curve and (f) Amplitude-frequency curve from S-transform for grid synchronization of wind generator with solar PV system

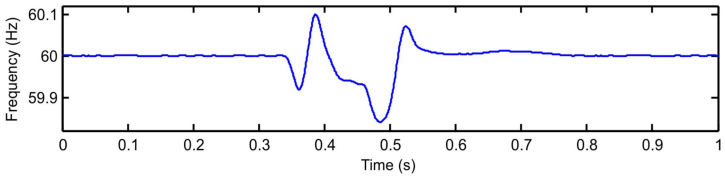

Figure 5.35 : Frequency variations with grid synchronization of wind generator with solar PV system

0.05 Hz.

Total harmonic distortions in voltage (THD_v) and current (THD_i) during operational events considered in this study are provided in Table 5.10. It is observed that THD_v and THD_i are below 5% for the events of outage and synchronization of solar/wind generators which is in accordance with IEEE-519 standard. However, the values of THD_v and THD_i are high for the islanding events. Islanding in the presence of both wind and solar generation significantly reduces the values of THD_v and THD_i. Actually, in the islanding events the test system operates as the microgrid and additional operating constraints are required for such events.

Maximum power frequency deviations from standard value of 60 Hz with wind generation of capacity 1.5 MW and solar PV generation of capacity 1 MW during all the events of study are provided in the Table 5.11. It has been observed that the maximum frequency deviations are observed with islanding event whereas during outage and synchronization events the changes are small. Power quality indexes during all the events of study are also provided in the Table 5.11. It has been observed that overall PQ is adversely affected in the case of islanding followed

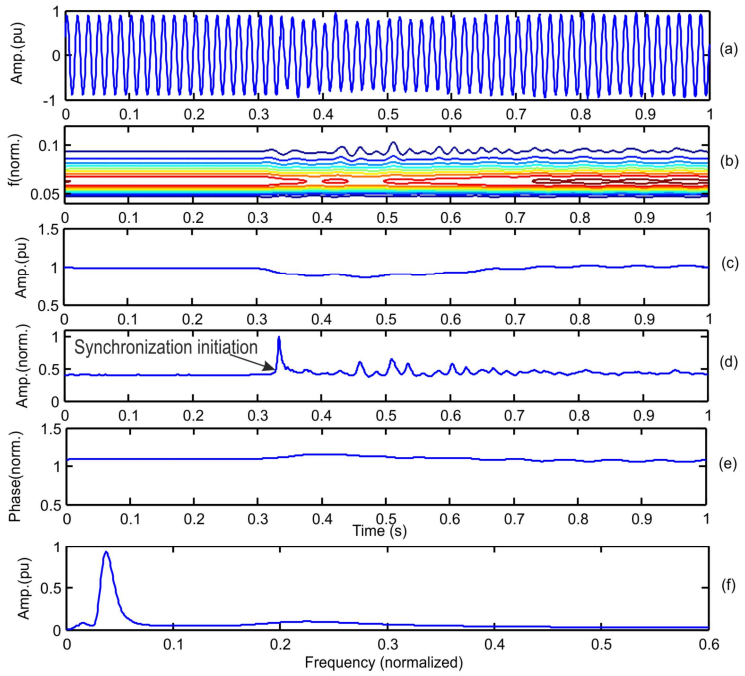

Figure 5.36 : (a) Voltage signal (b) S-contour (c) Amplitude curve (d) Sum of absolute values curve (e) Phase curve and (f) Amplitude-frequency curve from S-transform for grid synchronization of solar PV system with wind generation

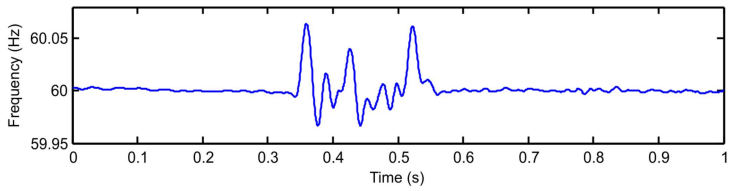

Figure 5.37 : Frequency variations with grid synchronization of solar PV system with wind generator

Table 5.10 : Total Harmonic Distortions of Voltage and Current in Hybrid Power System

Different cases of study	THD_v (%)	THD_i (%)
Islanding with wind energy	10.2843	14.6100
Islanding with solar energy	6.1512	13.0591
Islanding with wind and solar energy	1.1942	5.160
Outage of wind in the presence of solar energy	0.3189	1.7067
Outage of solar in the presence of wind energy	0.2544	0.7011
Outage of wind and solar simultaneously	0.1059	0.3909
Synchronization of wind in the presence of solar energy	0.2172	1.8516
Synchronization of solar in the presence of wind energy	0.2967	2.7612
Synchronization of wind and solar simultaneously	0.1557	0.5677

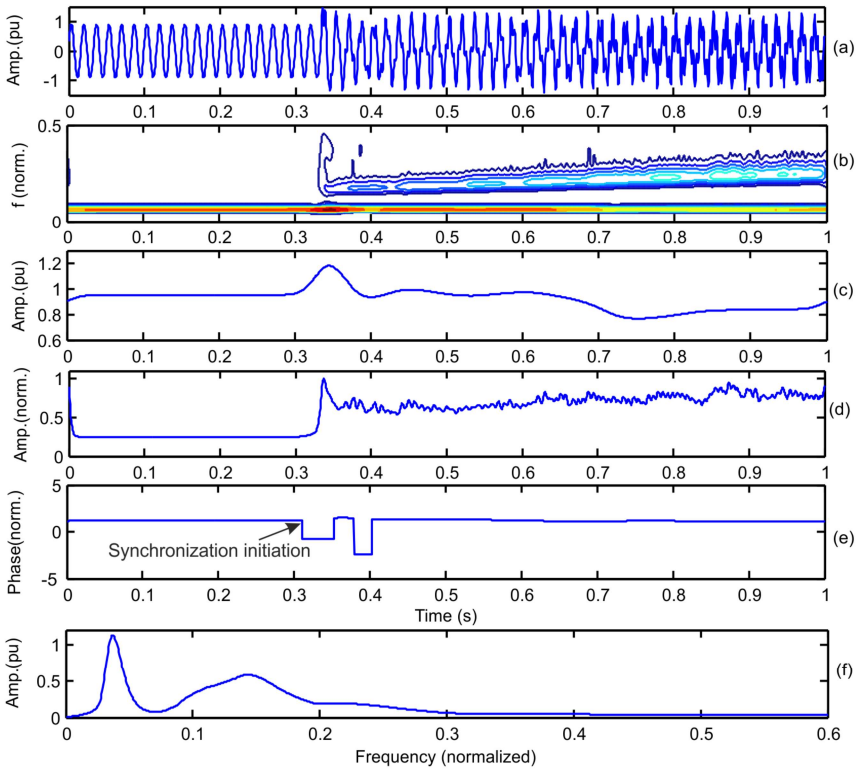

Figure 5.38 : (a) Voltage signal (b) *S*-contour (c) Amplitude curve (d) Sum of absolute values curve (e) Phase curve and (f) Amplitude-frequency curve from *S*-transform for simultaneous grid synchronization of wind and solar generators

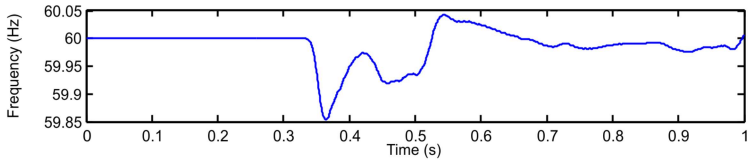

Figure 5.39 : Frequency variations with simultaneous grid synchronization of wind generator and solar PV system

by synchronization and outage. High power quality distortions are observed for simultaneous synchronization of both wind and solar PV generators.

5.8 DETECTION OF OPERATIONAL EVENTS: CASE STUDIES

This section details the detection of islanding, outage and synchronization in the hybrid power system. These operational events were simulated in the presence of (a) solar PV system (b) wind generator and (c) solar PV system and wind generator leading to a total of 9 scenarios labelled from C1 to C9 as illustrated in Table 5.12. Each scenario has been simulated with various incidence angles (0°, 30°, 60°, 90°, 120°and 150°) since the transients of the signal depends upon the angle of incidence of the waveform. Numerical values of the features F1 and F2 extracted for all the simulated events are provided in Table 5.12.

Table 5.11 : Maximum Frequency Deviations and Power Quality Index in Hybrid Power System

Different cases of study	Frequency deviation (Hz)	Power quality index
Islanding with wind energy	4	82.0289
Islanding with solar energy	8	116.1721
Islanding with wind and solar energy	4	78.3208
Outage of wind in the presence of solar energy	0.2	0.8071
Outage of solar in the presence of wind energy	0.15	0.8217
Outage of wind and solar simultaneously	0.18	0.7094
Synchronization of wind in the presence of solar energy	0.21	4.5698
Synchronization of solar in the presence of wind energy	0.06	6.8912
Synchronization of wind and solar simultaneously	0.15	9.9667

Fig. 5.40 presents the variations of maximum and minimum values of the feature F1 for the simulated events (C1 to C9). Feature F1 varies from 4.649 to 15.374 for the synchronization events (C7 to C9) whereas variation in the values of F1 for outage and synchronization events ranges from 22.414 to 37.490. Thus, the synchronization events (C7 to C9) can be discriminated from the outage and islanding events (C1 to C6) by selecting a threshold value of 20 (TH1) as illustrated in the Fig. 5.40.

Table 5.12 : Features of Negative Sequence Component of Voltage

Event	Class symbol	Value of feature F1 on the various incidence angles						Value of feature F2 on the various incidence angles					
		0°	30°	60°	90°	120°	150°	0°	30°	60°	90°	120°	150°
Islanding with wind energy	C1	29.940	30.279	30.504	30.816	30.581	30.303	161.002	162.391	163.547	165.184	163.870	162.592
Islanding with solar energy	C2	22.414	22.627	22.990	23.370	23.008	22.806	242.518	244.108	246.409	249.094	246.817	244.518
Islanding with wind and solar energy	C3	30.910	31.354	31.627	32.052	31.879	31.592	121.943	122.803	123.907	125.653	124.237	123.001
Outage of wind in the presence of solar energy	C4	34.721	35.110	35.605	36.007	35.817	35.394	3.669	3.807	3.903	4.106	3.921	3.833
Outage of solar in the presence of wind energy	C5	33.014	33.435	33.907	34.517	34.060	33.593	1.061	1.213	1.395	1.472	1.406	1.271
Outage of wind and solar simultaneously	C6	36.399	36.857	37.490	38.092	37.519	36.881	9.069	9.501	9.992	10.638	10.085	9.592
Synchronization of wind in the presence of solar energy	C7	13.331	13.576	13.908	14.359	13.972	13.602	176.233	177.812	178.916	180.131	178.995	177.902
Synchronization of solar in the presence of wind energy	C8	4.649	4.903	5.140	5.437	5.172	4.927	24.566	24.880	25.160	25.808	25.193	24.910
Synchronization of wind and solar simultaneously	C9	14.647	14.805	15.071	15.374	15.091	14.835	150.983	151.993	153.107	154.517	153.188	152.008

Fig. 5.41 presents the variations of maximum and minimum values of the feature F2 for the islanding and outage events (C1 to C6). Feature F2 varies from 121.943 to 246.409 for the islanding events (C1 to C3) whereas variation in the values of F2 ranges from 1.061 to 9.501 for the outage events (C4 to C6). Thus, the islanding events (C1 to C3) can be discriminated from the outage events (C4 to C6) by selecting a threshold value of 75 (TH2) as illustrated in the Fig. 5.41.

The proposed classification of the operational events has been illustrated by a flow chart shown in Fig. 5.5. Recognition of type of the RE sources present with the operational events is further investigated in the forthcoming subsections using the feature F2.

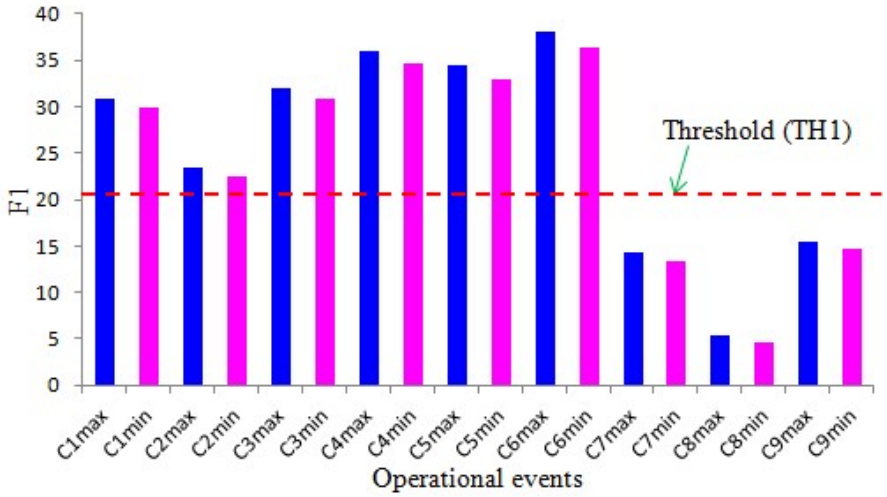

Figure 5.40 : Classification of synchronization events from other operational events

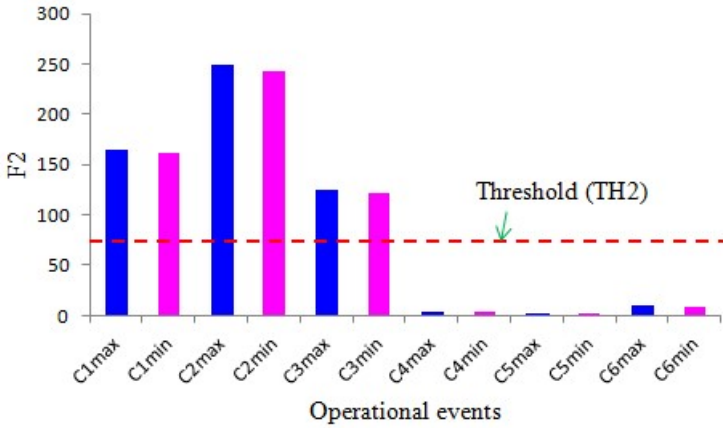

Figure 5.41 : Classification of islanding and outage operational events

5.8.1 Islanding

Fig. 5.42 presents the variations of maximum and minimum values of the feature F2 for the islanding events (C1 to C3). Feature F2 varies from 161.002 to 163.547 for islanding event in the presence of wind energy (C1). The same varies from 242.518 to 246.409 for the islanding event in the presence of solar energy (C2). Variations in the value of F2 ranges from 121.943 to 123.907 for the islanding event in the simultaneous presence of wind and solar energy (C3). From the Fig. 5.42, it can be observed that the nature of RE sources present during the islanding events (C1 to C3) can be detected by selecting threshold values of 190 (THI1) and 140 (THI2). Thus, feature F2<THI2 indicates the presence of both wind and solar energy. F2>THI1 indicates the presence of solar energy whereas the value of F2 between THI1 and THI2 (THI1 >F2 >THI2) indicates the presence of wind energy.

5.8.2 Outage of RE Generators

Fig. 5.43 presents the variations of maximum and minimum values of the feature F2 for the outage events (C4 to C6). Feature F2 varies from 3.669 to 4.106 for outage of wind generator in the

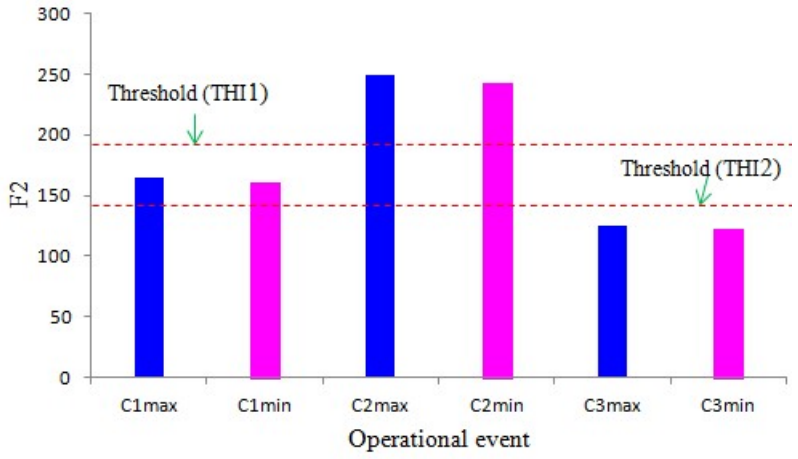

Figure 5.42 : Variance plots for detection of islanding events

presence of solar PV system (C4). The same varies from 1.061 to 1.472 for outage of solar PV system in the presence of wind generator (C5). Variations in the value of F2 ranges from 9.069 to 10.6387 for the event of simultaneous outage of both wind generator and solar PV system (C6). From Fig. 5.43, it can be observed that the nature of RE sources present during the outage events (C4 to C6) can be detected by selecting threshold values of 5.5 (THO1) and 2.5 (THO2). Thus, feature F2>THO1 indicates simultaneous outage of both wind and solar energy. F2<THO2 indicates the outage of solar PV system in the presence of wind energy whereas the value of F2 between THO1 and THO2 (THO1>F2>THO2) indicates the outage of wind generator in the presence of solar energy.

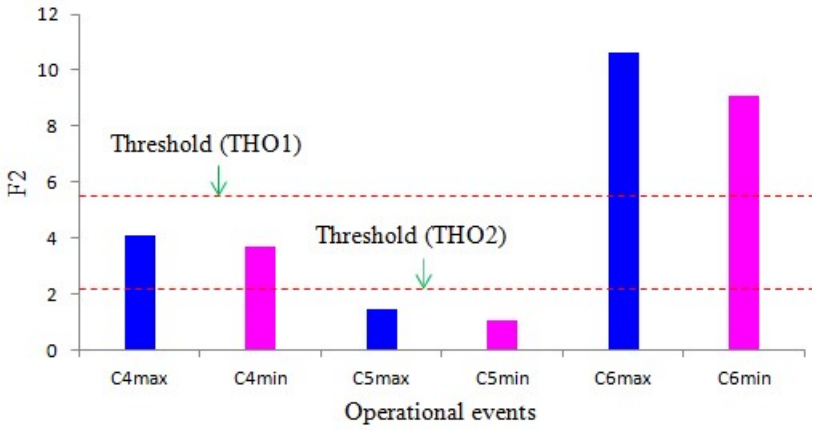

Figure 5.43 : Variance plots for detection of outage events

5.8.3 Grid Synchronization of RE Generators

Fig. 5.44 presents the variations of maximum and minimum values of the feature F2 for the synchronization events (C7 to C9). Feature F2 varies from 176.233 to 180.131 for synchronization of wind generator in the presence of solar PV system (C7). The same varies from 24.566 to 25.808 for synchronization of solar PV system in the presence of wind generator (C8). Variations in the value of F2 ranges from 150.983 to 154.517 for the event of simultaneous synchronization of both wind generator and solar PV system (C9). From Fig. 5.44, it can be observed that the nature of RE sources present during the synchronization events can be detected by selecting threshold values of 162 (THS1) and 85 (THS2). Thus, feature F2>THS1 indicates the synchronization of wind generator

in the presence of solar energy. F2<THS2 indicates the synchronization of solar PV system in the presence of wind energy whereas the value of F2 between THS1 and THS2 (THS1>F2>THS2) indicates the simultaneous synchronization of wind generator and solar PV system.

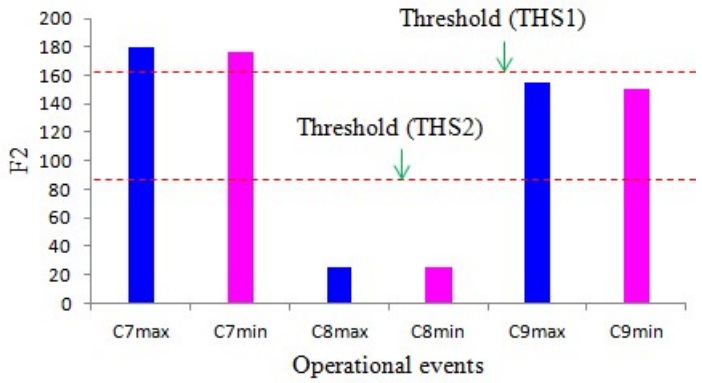

Figure 5.44 : Variance plots for detection of synchronization events

5.9 TESTING OF RESULTS IN REAL TIME USING RTDS

Testing of the results in real time using RTDS has been carried out using the experimental set-up described in the section 3.11. Error between the real time and simulation results calculated using equation (3.11). The real time results obtained using the RTDS are illustrated in the following subsections.

5.9.1 Wind Energy System

The *S*-transform based plots of real time results related to outage of wind generator are shown in Fig. 5.45. These results are very close to the simulation results. It has been observed that real time results are very close to the simulation results. Percentage error between real time results and simulation results is below 2%. Therefore, the proposed *S*-transform based algorithm proved to be effective for investigation of power quality disturbances associated with grid integrated wind power generators.

5.9.2 Solar PV System

Real time results of voltage signal during grid synchronization of solar PV system and related *S*-transform based plots are shown in Fig. 5.46. These results are very close to the respective simulation results. The comparison of real time results with the simulation results has been carried out based on the power quality index and an error between these results is obtained. It has been observed that real time results are very close to the simulation results. Percentage error in the value of power quality index is below 2%. Therefore, the proposed *S*-transform based algorithm has been proved to be effective for investigation of power quality disturbances associated with grid operations of solar PV system.

5.9.3 Hybrid Power System

Real time results of voltage signal during outage of solar PV generator in the presence of wind power generation in the hybrid power system and related *S*-transform based plots are shown in Fig. 5.47. These results are very close to respective simulation results. Real time results for all the cases of study are compared with the respective simulation results using the proposed power quality index and an error between these results is obtained. It has been observed that real time results are very close to simulation results. Percentage error in the value of power quality index

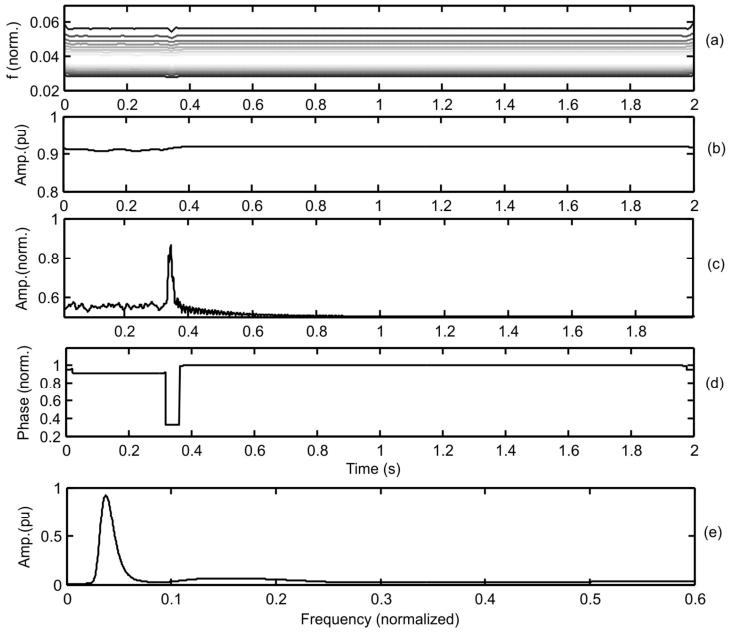

Figure 5.45 : Real time results (a) Frequency contour (b) Amplitude curve (c) Sum of absolute values curve (d) Phase curve (e) Amplitude-frequency curve from S-transform for outage of wind generator

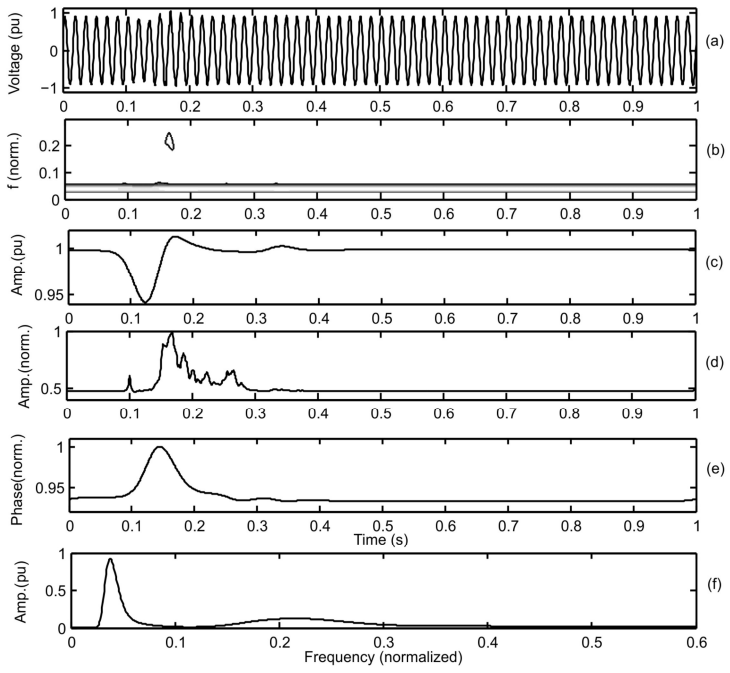

Figure 5.46 : Real time results (a) Voltage signal at PCC (b) Frequency contour (c) Amplitude curve (d) Sum of absolute values curve (e) Phase curve (f) Amplitude-frequency curve from *S*-transform for grid synchronization of solar PV system

is below 2% for islanding and outage events whereas this error is below 4% for synchronization events. Therefore, proposed *S*-transform based algorithm has been proved to be effective in the detection of Islanding and power quality disturbances in the RE sources based hybrid power system.

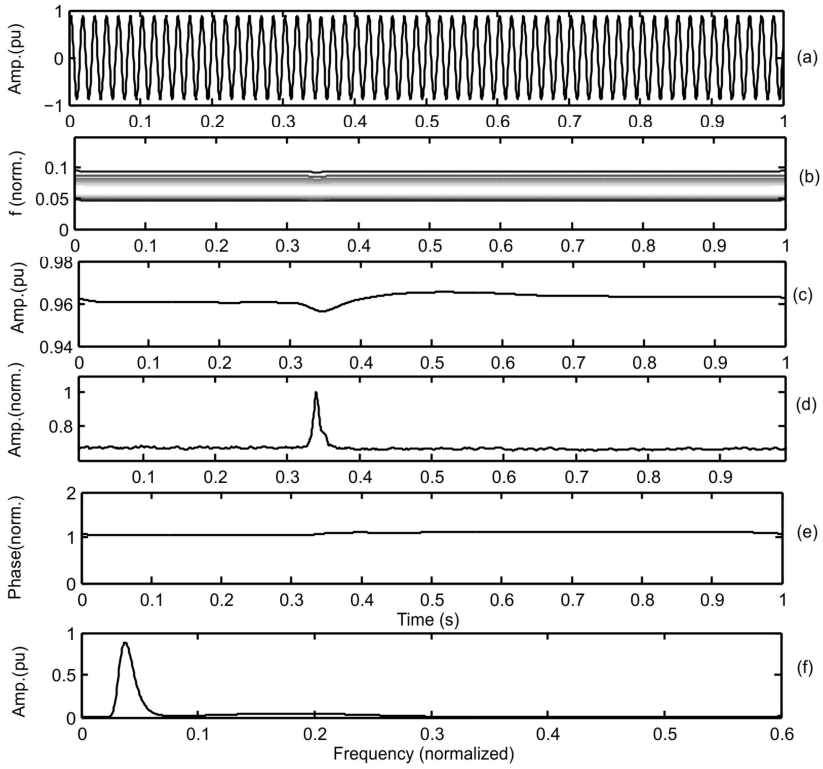

Figure 5.47 : Real time results (a) Voltage signal (b) Frequency contour (c) Amplitude curve (d) Sum of absolute values curve (e) Phase curve and (f) Amplitude-frequency curve from *S*-transform for outage of solar PV generator in the presence of wind generation

5.10 CONCLUSIONS

Operational events such as islanding, outage of wind/solar generators and grid synchronization of wind/solar generators are detected utilizing the *S*-transform based features and Fuzzy C-means clustering with the help of negative sequence component of voltage. Dynamic simulation results related to variations in the grid voltage, active power supplied by wind generator, reactive power supplied by wind generator and frequency during the event of synchronization of wind generator are provided in Fig. 5.48. Dynamic simulation results related to variations in the grid voltage, active power supplied by wind generator, reactive power supplied by wind generator and frequency during the event of outage of wind generator are provided in Fig. 5.49. Dynamic simulation results related to variations in the grid voltage, active power supplied by wind generator, reactive power supplied by wind generator and frequency during the event of islanding in the presence of wind generation are provided in Fig. 5.50.

The major challenges of the power quality with renewable energy include solar insolation changes in a fraction of second resulting in abrupt change in the power output of solar plant affecting the quality of power, variation in wind speed also changes the power generation of wind plant affecting quality of power, outage of plants affect the quality of power, power electronic interface converters and their control schemes are different for different types of RE power plants which

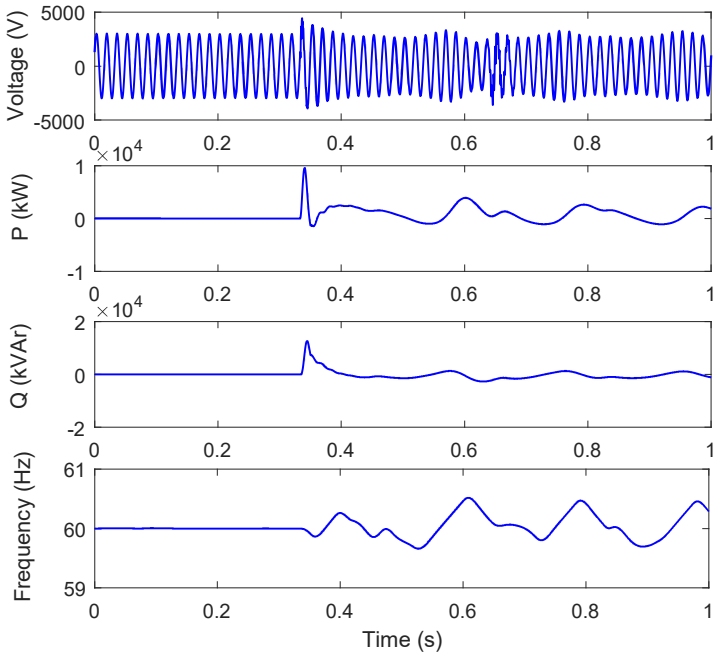

Figure 5.48 : Dynamic results of synchronization event of wind generator (a) Voltage (b) Active power supplied by wind generator (c) Reactive power supplied by wind generator and (d) Frequency variation

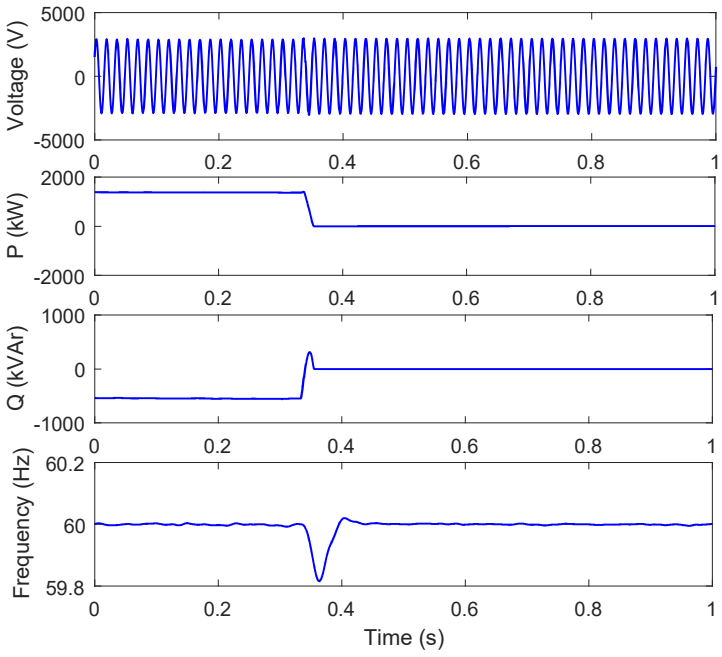

Figure 5.49 : Dynamic results of outage event of wind generator (a) Voltage (b) Active power supplied by wind generator (c) Reactive power supplied by wind generator and (d) Frequency variation

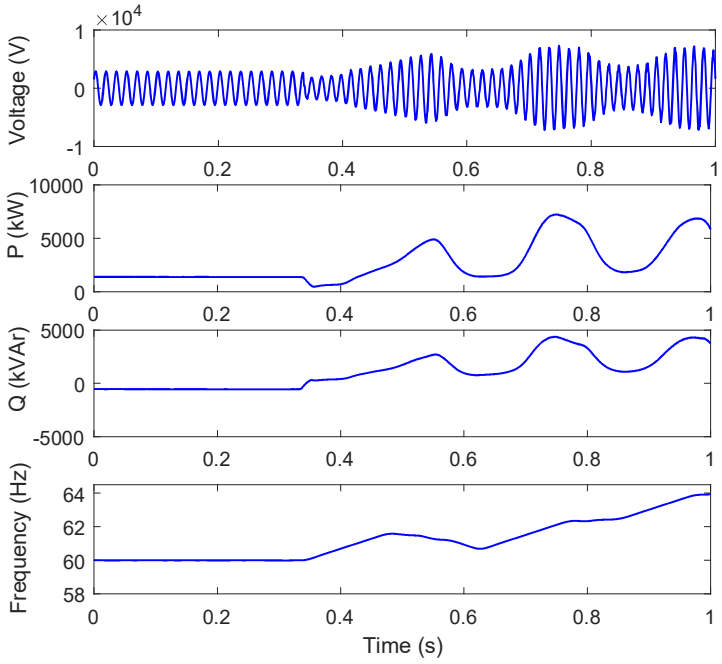

Figure 5.50 : Dynamic results of islanding event in the presence of wind generator (a) Voltage (b) Active power supplied by wind generator (c) Reactive power supplied by wind generator and (d) Frequency variation

results in different types of PQ problems and a single methodology is not available for detection and classification of all types of PQ events in the presence of RE sources. The presented research work helps to overcome these major challenges of the power quality with renewable energy.

Power quality disturbances associated with the events such as islanding, outage of wind/solar generators and grid synchronization of wind/solar generators have been investigated using the *S*-transform, FFT and proposed power quality index. It can be concluded that the proposed algorithm effectively detects the events such as islanding, outage of wind/solar generators, and grid synchronization of wind/solar generators in the RE sources based power system. Power quality disturbances such as voltage fluctuations with sag and swell, flicker, transients and power frequency deviations are detected with grid synchronization of wind generator. Voltage swell, low magnitude transients and power frequency deviations are associated with outage of the wind generator. High magnitude voltage sag and swell, oscillatory transient, harmonic transients, flicker and power frequency variations have been detected with islanding of test system from the utility grid. Low magnitude voltage fluctuations, flicker and frequency variations are observed with the wind speed variations. Power quality index indicates that overall power quality deteriorates with increase in the wind energy penetration level. Maximum effect is observed with the islanding followed with the synchronization, wind speed variations and minimum with the outage of wind generator. It has been observed that the PQ disturbances such as voltage fluctuations, sag, swell, flicker and transients are present with grid synchronization of the solar PV generator. Synchronization increases voltage level in the feeder whereas the voltage level decreases with the outage of solar PV generator. An impulsive transient is detected with outage event. High frequency transients and flickers have not been detected with the outage. Voltage fluctuations with decrease in the voltage have been detected with the abrupt change in solar insolation. Low frequency magnitude transients and flicker have also been detected with the abrupt change in solar insolation. Power frequency variations have been observed with all the cases of study having maximum effect with

the change in solar insolation and minimum effect with the outage. PQ index indicates that power quality deteriorates with increase in penetration level of the solar PV energy into the utility grid and maximum effect is observed with the synchronization followed by change in solar insolation and minimum with outage. The proposed algorithm can effectively be used to recognize the PQ events associated with operational events in the hybrid power system. The high values of THD_v and THD_i are observed with the islanding events. However, the values are below 5% for the outage and synchronization events. Power quality index indicates that the power quality is adversely affected with the islanding event. However, with the outage and synchronization events power disturbances are acceptable whereas it is quite high with the synchronization events as compared to the outage events.

...